JOURNAL OF GUIDANCE, CONTROL, AND DYNAMICS
Vol. 31, No. 2, March–April 2008

Coordinated Standoff Tracking of Moving Targets Using Lyapunov Guidance Vector Fields

Eric W. Frew*
University of Colorado, Boulder, Colorado 80302
Dale A. Lawrence†
University of Colorado, Boulder, Colorado 80302
and
Steve Morris‡
MLB Company, Mountain View, California 94043

DOI: 10.2514/1.30507

This paper presents a control structure for cooperative stand-off line-of-sight tracking of a moving target by a team of unmanned aircraft based on a Lyapunov guidance vector field that produces stable convergence to a circling limit cycle behavior. A guidance vector field is designed for a stationary target and then modified with a correction term that accounts for a moving target and constant background wind. Cooperative tracking by multiple unmanned aircraft is achieved through additional phasing, also with a Lyapunov stability analysis. Convoy protection, in which the unmanned aircraft must scout an area ahead of the moving target, is performed by extending the cooperative stand-off line-of-sight limit cycle attractor along the direction of travel. Simulation results demonstrate the behavior of the algorithms as well as the improvement that results from cooperation. Finally, simulations of a larger cooperative search, acquisition, and tracking scenario are described that illustrate the use of the cooperative stand-off line-of-sight and convoy protection controllers in a realistic application.

Nomenclature

$CSAT$	=	cooperative search, acquisition, and tracking
$CSLOS$	=	cooperative stand-off line of sight
D_b	=	rear elongation for convoy protection pattern
D_f	=	forward elongation for convoy protection pattern
FCS	=	flight control system
f_{off}	=	fractional offset for convoy protection pattern
GV	=	ground vehicle
$\dot{h}_{\max}$	=	maximum aircraft climb rate
K	=	control gain
LOS	=	line of sight
m	=	number of targets in coordination optimization algorithm
n	=	number of UA in coordination optimization algorithm
$\mathbf{p}_t$	=	center of desired loiter circle
R_t	=	turn radius for convoy protection pattern
(r, θ)	=	position of UA in polar coordinates centered on moving target
r_d	=	commanded stand-off distance
$SLOS$	=	stand-off line of sight
t_{ij}	=	time to intercept estimate in coordination optimization algorithm
UA	=	unmanned aircraft
UAS	=	unmanned aircraft system
U_1, U_2, U_3	=	admissible air speed, turn rate, and climb rate sets
$v_{\min}, v_{\max}$	=	minimum and maximum air speed
(v_0, h_0)	=	constant speed and altitude commands
(u_1, u_2, u_3)	=	commanded speed, turning rate, and altitude
V, V_p	=	Lyapunov functions for loitering and phasing
W_x, W_y	=	background wind velocity
$\{X_{11}, X_{12}, X_{21}, X_{22}\}$	=	corner points for convoy protection pattern
(x, y, h)	=	components of the three-dimensional UA inertial position
$(\dot{x}_d, \dot{y}_d)$	=	guidance vector field
x_{ij}	=	binary assignment variable in coordination optimization algorithm
$(\dot{x}_r, \dot{y}_r)$	=	Cartesian coordinates of velocity of UA relative to target
(x_t, y_t)	=	components of $\mathbf{p}_t$
$(\dot{x}_t, \dot{y}_t)$	=	Cartesian coordinates of target vehicle inertial velocity components
η	=	relative course angle
(θ_1, θ_2)	=	angles of two UA on loiter circle in cooperative tracking
χ	=	course angle
ψ, ψ_d	=	aircraft heading and desired heading
$\omega_{\max}$	=	maximum aircraft turn rate

Received 16 February 2007; revision received 20 September 2007; accepted for publication 21 September 2007.

*Assistant Professor, Aerospace Engineering Sciences. AIAA Member.
†Associate Professor, Aerospace Engineering Sciences. AIAA Senior Member.
‡President, 2551 Casey Avenue, Suite B.

I. Introduction

TEAMS of low-cost unmanned aircraft (UA) with autonomous behaviors will be capable of performing inexpensive, persistent, distributed sensing functions. One application of interest is the use of UA teams to perform cooperative tracking of moving surface (land or sea) targets, particularly in the context of area surveillance, cooperative patrol, and convoy protection. In many scenarios, the UA must reduce their exposure to threats and conduct operations in a stealthy manner. The development of stand-off line-of-sight (SLOS) trajectories allow the UA to track moving surface

targets whereas maintaining sensor coverage and remaining outside a critical threat range [1,2]. Team tracking of moving surface vehicles can improve sensor coverage when the target vehicle is uncooperative, or is highly agile, such that estimates of its position and velocity are poor. The idea is to distribute UA in a stand-off pattern, and so that unpredicted changes in vehicle motion can be observed and followed by the UA in the most advantageous position and so that errors in the geolocation of moving targets can be improved by independent sensor information.

The basic moving surface target tracking mission is to provide continuous live sensing (typically imagery) from around and ahead of friendly, adversarial, or unidentified (i.e., could be friendly or adversarial) targets. Although the instantaneous location and speed of friendly vehicles may be available to the UA team, here we assume all targets are noncooperative in the sense that their routes or intentions are unknown to the UA. We consider fixed-wing vehicles, characterized by higher efficiency flight and longer duration, but with narrower restrictions on air speed compared with rotorcraft. Because minimum air speed is typically larger than surface vehicle speed, UA must orbit around the target to maintain sensor contact; hence, leader/follower SLOS tracking that matches the target velocity at a fixed stand off [3] is not workable. For friendly surface convoys, the UA must search sufficiently far ahead and to the sides of the convoy to give ample warning of road and threat status. Likewise, UA must be able to orbit unknown moving targets at a safe horizontal stand-off distance to ascertain their threat level or to maintain optimum sensor resolution and field of view for accurate target geolocalization.

The tracking of moving surface targets is often complicated by loss of sensor (image) tracking resulting from failure of the UA to anticipate the ground target turn direction, lack of UA maneuvering agility, and mechanical limits of the sensor's gimbal system. Ground vehicles can outmaneuver most fixed-wing UA because the UA airspeed is more constrained than the ground vehicle, which can stop quickly, and the UA has a relatively large turn radius. A gimbal mounted sensor system reduces the impact of the maneuvering disparities between the vehicles, but there are significant trade offs in what the gimbal sensor can accomplish relative to the cost of the UA. For example, a UA with a highly stabilized sensor system to account for maneuvering and disturbances acting on the aircraft with long-range zoom capability can fly at a farther slant range to the image target and thereby minimize the total range of gimbal angle excursions needed to track the target (e.g., the target will typically stay on one side of the aircraft). This type of system is typically larger and more costly than most small UA and requires a large infrastructure to support it. Flying high or far away from the target is not always an option because of obstacles that may block the line of sight and weather (clouds, fog, etc.) that may prevent viewing from a great distance. Flying closer to the target requires a larger range of motion from the gimbal for tracking, but reduces the need for exceptional gimbal stability and therefore reduces system size and cost. Ultimately, a solution that uses teams of UA to keep the target in view is preferred because this allows low-cost, less-agile UA to perform the mission, maintaining coverage of the region even if any one aircraft loses track. Additional challenges that can be addressed by teams of UA performing cooperative stand-off line-of-sight (CSLOS) tracking include: maintaining RF communication to the ground station by forming RF relays, tracking physically large moving targets (e.g., convoys), and enabling multiple simultaneous views of targets for stereo or mosaic imaging.

A. Related Work

Inner-loop flight control of unmanned aircraft typically yield closed-loop dynamics that provide good tracking of altitude, heading, and speed reference commands; hence, constant altitude operation is well approximated by a planar kinematic unicycle model. This is the basis for a variety of guidance and control schemes. Cooperative, *non*-stand-off tracking of a moving ground vehicle has been demonstrated for convoy protection applications [4,5]. In these applications, the ground target is friendly, and UA trajectories are designed that periodically fly directly over the moving vehicle as well as loop away horizontally to provide surveillance of its surrounding environment. Multiple aircraft are coordinated through a high level task allocation algorithm that assigns vehicles to predetermined classes of orbits, and relative phasing between orbits is obtained by a timing optimization algorithm that adjusts orbit pattern lengths to achieve the surface vehicle overflight timing. The controlling phase is not attempted throughout the orbits.

Cooperative stand-off work can be grouped into two main classes. The first is stability oriented, in which control laws are sought that produce asymptotic stability to desired reference states. The second is behavior oriented, in which the motion enroute to the reference state is also part of the design process. The approach presented here is in the latter category.

The stability-oriented class includes path-tracking approaches in which a stand-off orbiting path is defined, and a virtual target on the path is specified for the UA to track [6,7]. In the "good helmsman" path-following [2,7,8] approach, the path-following problem is formulated in the Serret–Frenet frame from differential geometry. Control is designed to regulate the cross-track (lateral) error and course heading error to zero in this frame by calculating an intercept course that varies with the cross-track distance. Two-vehicle cooperative stand-off tracking of moving targets [2] is achieved by varying speed commands to space two unmanned aircraft around this reference path. The necessary aircraft speeds needed to maintain relative spacing about a moving target in the presence of background wind typically exceed the flight envelope of most unmanned aircraft, leading [2,8] to an outer loop that varies the commanded stand-off distance and relative separation angles as functions of target speed, wind speed, and aircraft clock angles. Local stability is shown, but global behavior is complicated by nonuniqueness of computed virtual targets on the path (e.g., as closest points on the path or with a specified look-ahead distance).

A second method uses sliding mode control in conjunction with a cooperative control Lyapunov function (CCLF) that is expressed in terms of the error of a two-UA team from a desired configuration [9]. The CCLF presented in [9] specifies the desired geometrical team configuration through the combination of individual vehicles terms (e.g., the distance from the desired stand-off radius and a joint term based on the desired relative separation distance between vehicles, which is a function of the desired geometry). The time rate of change of the CCLF is prescribed to be negative definite through a control law similar to sliding mode control.

Global stability results have been obtained in collective motion approaches for multiple vehicles [10–13]. There, vehicle speed is constant, and simple relative position and heading feedback laws between all vehicles are specified that result in interesting collective stability results, such as convergence to equally spaced motion on a circular orbit about a fixed target [10,12,13]. An extension [11] addresses moving targets with constant speed UA, resulting in deviation of UA from a fixed stand-off radius, although they periodically return. Collective motion control for trajectory tracking only applies to symmetric spacing of at least three vehicles. A modification of the collective control approach to stand-off tracking by two vehicles is presented in [8], but no stability results are provided.

The behavior-oriented class of orbiting CSLOS control systems explicitly specify the motion behavior toward the desired orbit and then implement control to achieve this motion. This separates the guidance and control functions. A guidance vector field is constructed that provides the desired motion velocity of the UA at any position in the domain, and this velocity is used as the reference heading and speed for the lower-level control system to track. This approach stems from potential field work in mobile robotics [14,15] producing streamlines from scalar gradients but adds circulation (curl) to the vector field to produce orbiting UA behavior. This paper builds on the idea from [16] for a single vehicle, which is similar to later work [10,17]. Here we add compensation for wind and target motion and coordination terms for multiple vehicles. This results in a control law that is globally stable to specified angular spacing on an

orbit about the target, but also provides guaranteed stand-off distance from a moving target while satisfying UA airspeed constraints.

A similar vector field approach for regulating to a circular loiter pattern is given in [17]. A vector field is described based on the desired course angle of the aircraft (i.e., the direction of the aircraft velocity vector in a fixed global reference frame), and a sliding mode controller is used to bring the aircraft on to the vector field. Stability of this approach is given for a single aircraft loitering about a fixed target point. Although the system described in [17] is robust to unknown background winds, this fact comes from assumptions about the low-level control of the system. In particular, the analysis assumes that a low-level autopilot provides the ability to directly control course angle rate in the presence of any wind, which requires high-gain inner-loop control. The analysis in [17] does not consider the effects of a moving target or cooperative tracking. Furthermore, several subtle details such as singularity of the vector field at the origin (target location) are not discussed.

The good helmsman coordination approach [2], collective motion control for trajectory tracking [11], a model predictive controller (MPC), and an algorithm similar to the guidance vector field approach described in this paper are compared in several two-UA tracking scenarios in the presence of wind [8]. The good helmsman control and the guidance vector field perform well for each test case, including tracking a maneuvering target and in an unknown wind. The good helmsman control regulates the desired angular spacing the best at the expense of increased range from the target whereas the guidance vector field approach maintains the specified (minimum) stand-off distance at the expense of phase spacing error. Whereas the performance of each controller was evaluated against a desired tracking configuration, the effects of the deviation from this configuration on the underlying objective (e.g., target geo-localization), depend on additional variables such as the sensor characteristics [18] and thus direct comparison of the different approaches is incomplete. The collective motion controller and model predictive controller performed well tracking moving targets but demonstrated poor robustness to an unknown background wind.

The contribution of this work is a distributed control architecture for cooperative stand-off tracking of a moving target in the presence of wind. A new cascaded control approach is described that decomposes the solution into three layers: the highest layer uses speed control to coordinate UA spacing relative to a moving target, the second layer specifies the desired aircraft velocity at every point in the environment through a guidance vector field to bring the UA onto a loiter pattern about the target, and the third layer regulates the aircraft motion to the resultant desired path. Stability analysis is provided in this article to show that the vector field is essentially globally stable (except at the origin) and that any input brings the system off the origin into the stable domain. This analysis considers both singularity in the vector field at the origin and wrapping effects because of desired motion on the special orthogonal group on a circle. Finally, unlike previous work [17], we consider the impact of unknown target and wind velocities as disturbances in the motion that results from following the vector field.

B. Control Architecture

The control strategy presented here is motivated by a hierarchical approach to the autonomous coordination of multiple unmanned aircraft performing different reconnaissance and surveillance missions. We assume the presence of a low-level flight control system that controls the aerodynamic surfaces of the aircraft to accurately track speed, turn rate, and climb rate commands from the guidance layer and a high level coordination layer that assigns individual vehicles to different tasks. The focus of this paper is on the guidance layer, but an illustration of the integration of guidance with multitask coordination is also provided.

The guidance layer developed here consists of two sublayers (Fig. 1) based on steering control and speed control, respectively. The first (lower) sublayer uses a vector field approach to steer individual vehicles onto desired orbiting CSLOS patterns. The inputs to this layer include the aircraft position and velocity, target position and velocity, desired stand-off radius, and commanded airspeed, whereas the output consists of a turn rate command. The second sublayer regulates the relative phase of the aircraft about the target position. Inputs to this layer include the aircraft and target positions (velocities are not needed), the desired angular (phase) separation relative to the target, and the phase angle between each UA and the target. The output is the speed command for each vehicle. Intervehicle communication is minimal for this control approach, because the only information that must be shared is the phase angle of each aircraft relative to the target. For this work, we do not address target estimation. We assume estimated target position and velocity are the same for each vehicle. Although estimates could be generated through distributed, decentralized, or individual estimators, we have depicted a centralized target estimation subsystem in Fig. 1.

Individual aircraft tracking control is based on guidance laws developed in using the Lyapunov stability theory. Instead of constructing Lyapunov functions to analyze stability of a given control law, families of vector fields are constructed to produce the desired Lyapunov function (and hence desired vehicle) behavior. This process begins with the construction of a Lyapunov function with desired properties as zero level sets, and with "energy" penalty elsewhere. Then, guidance laws are stipulated that produce time derivatives of this function, which are nonpositive, ensuring global attraction of the UA state to the desired behavior. Unlike similar potential function approaches [15,19–23], these laws explicitly produce limit cycle behavior, which enables the UA to safely maintain adequate airspeed as they track targets on the ground. A reference tracking controller commands speed and turn rate to cause the aircraft to follow the guidance vector field.

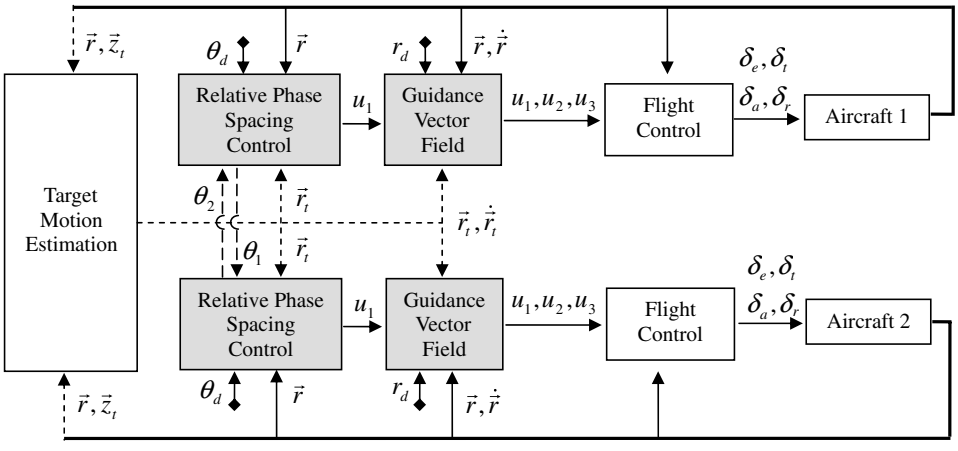

Fig. 1 Control architecture for cooperative stand-off tracking of a moving ground target by two unmanned aircraft. Solid lines represent data generated and used onboard each vehicle, whereas dashed lines indicate data that must be communicated.

A modification is made to this globally stable loitering behavior to produce robust tracking of moving targets. Assuming the UA starts outside the desired loiter pattern and the target moves at a constant velocity with speed less than the aircraft airspeed, this modification guarantees that the specified minimum stand-off distance constraint is never violated while maintaining the specified airspeed of the aircraft. When known, the velocity of the target and the background wind are incorporated into the tracking controller as a correction to the guidance vector derived from the Lyapunov approach. This correction term ensures that the airspeed of the aircraft matches the commanded value without changing the global stability of the guidance vector field.

The strengths of this Lyapunov guidance vector field approach compared with the good helmsman path following and collective motion control algorithms are fourfold. First, the guidance vector field approach provides provable global stability (except for the single state in which the aircraft position matches the target position) to the desired loiter circle behavior. As mentioned before, the collective motion control algorithms require three or more vehicles for reference tracking by the collective centroid, and do not regulate to moving loiter circle patterns. Likewise, path following (with or without good helmsman behavior) based on the Serret–Frenet frame can suffer from position ambiguities (i.e., there can be multiple points on the desired path that are equidistant from the vehicle position) and therefore only provide local stability guarantees. Second, feasibility of the desired vector field motion in terms of turn rate (curvature) constraints can be guaranteed for static targets as long as the desired loiter circle is feasible. Neither the collective motion algorithms nor good helmsman tracking controllers address path feasibility. Third, stand-off tracking is guaranteed for known background wind and moving target velocity (up to specified limits) while maintaining the desired air speed of the unmanned aircraft. A correction term is derived for the vector field approach that does not change the global stability properties of the algorithm. Fourth, the Lyapunov energy function used to define the vector field control is a convenient measure of the time to reach the desired loiter pattern for static targets. This allows for abstraction of the guidance control layer by higher level coordination schemes that can generate optimal group behavior from simple assignment algorithms. For moving targets, the global stability of the vector field approach also allows for some abstraction of the guidance control layer by a group coordination layer (i.e., the vehicle motion can be thought of as residing on the circle after a known time for the purposes of higher-level planning).

Multiple vehicle coordination is achieved by controlling the relative phase angle between the aircraft as they circle around the target. A second Lyapunov function is used to derive speed commands for each aircraft to space them about the loiter circle defined by the first controller. The desired phase spacing can be chosen based on the objective of the cooperative tracking mission. Uniform spacing (i.e., 180 deg phase separation) of two aircraft reduces the ability of the ground target to evade the group by increasing the probability that at least one of the aircraft will be in a position to adequately respond to an evasion maneuver, whereas a phasing of 90 deg is optimal for cooperative geolocalization [18,24]. Unlike the outer loop control in [2,8] that varies the commanded stand-off distance and relative separation angles as functions of target speed, wind speed, and aircraft clock angles, we assume that maintaining minimum stand-off separation between the UA and target is preferred to maintaining desired/optimal phase spacing [18].

The guidance layer algorithms are developed in this paper for the specific target tracking application, but can be used in more general cooperative control frameworks as well. The general cooperative control philosophy that motivates development of the guidance vector field approach stresses simple but provably stable and robust controllers at each layer in a control hierarchy. Abstraction of lower-layer controllers by higher-level processes can rely on these stability properties to simplify controllers at other levels. For example, the Lyapunov function used in Sec. III.A to prove the global stability of the guidance vector fields can serve as a measure of relative time to target by an algorithm assigning multiple aircraft running the same underlying guidance control to different tasks. Likewise, distribution or coverage control for teams of vehicles is simplified by working with only the center points of the loiter circles. In each case, guaranteed low-level performance is abstracted away to provide a simplified problem to the higher layer algorithms. Example applications that have used the guidance vector field approach described in this paper include cooperative, search, acquisition, and tracking by teams of unmanned aircraft (see Sec. IV); distributed toxic plume tracking by micro air vehicles [25]; and controlled mobility in multihop communication networks [26].

The remainder of this paper is presented as follows. Section II presents the dynamic model used for control law development at the guidance level. Section III describes stand-off line-of-sight tracking control that maintains safe separation distance from a target object. The basic algorithm is presented for a stationary target in the absence of wind and then a modification is described that accounts for known constant target velocity and known constant background wind. Section IV extends the SLOS tracking controller to multiple cooperating vehicles. Finally, Sec. V illustrates how vehicles endowed with Lyapunov CSLOS guidance laws can be coordinated simply at higher levels to provide sophisticated team capabilities. This simulation uses a CSAT coordination architecture to coordinate a team of six UA surveying an area that contains three moving ground targets.

II. System Models

This work assumes UA are equipped with a low-level flight control system (FCS) that provides roll, pitch, and yaw stability of the aircraft as well as velocity tracking and altitude-hold functions. For aircraft guidance, the FCS accepts explicit speed, climb rate, and turn rate commands. Using this command structure, the system model presented to the guidance layer is a kinematic model:

$$\dot{x} = u_1 \cdot \cos\psi + W_x \qquad \dot{y} = u_1 \cdot \sin\psi + W_y \qquad \dot{\psi} = u_2 \qquad \dot{h} = u_3 \tag{1}$$

where $[x, y, h]^T \in \Re^3$ is the three-dimensional inertial position of the aircraft, $\psi \in [0, 2\pi)$ is the aircraft heading (90 deg minus the compass heading), $[W_x, W_y]^T \in \Re^2$ are the components of the steady background wind velocity (Fig. 2), and $u_i \in U_i$ $i = 1, 2, 3$ are, respectively, the commanded air speed (m/sec), turning rate (rad/sec), and climb rate (m/sec), which are constrained to the limits

$$\begin{aligned} U_1 &= \{u_1 \in \Re | 0 < v_{\min} \le u_1 \le v_{\max}\} \\ U_2 &= \{u_2 \in \Re | |u_2| \le \omega_{\max}\} \qquad U_3 = \{u_3 \in \Re | |u_3| \le \dot{h}_{\max}\} \end{aligned} \tag{2}$$

For this work, the climb rate command is given by simple proportional feedback $u_3 = -k_h(h - h_o)$, where h_o is the task-specified altitude.

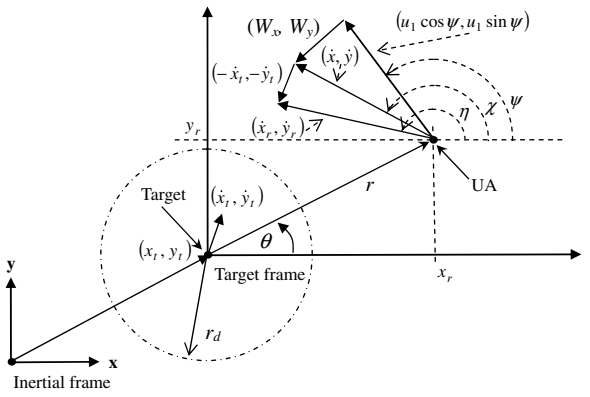

Fig. 2 Tracking geometry with the ground target of interest at the origin of the *target frame*.

An alternative formulation of the kinematic model of Eq. (1) uses the inertial speed V and course angle χ. If ψ_w is the wind direction, then $W_x = W\cos\psi_w$ and $W_y = W\sin\psi_w$ and the new formulation is

$$\dot{x} = V\cos\chi \qquad \dot{y} = V\sin\chi \qquad \dot{\chi} = k_\chi(\psi)\cdot\dot{\psi} = k_\chi(\psi)\cdot u_2 \tag{3}$$

where if u_1, ψ_w, and W are constant,

$$\begin{aligned} V^2 &= u_1^2 + W^2 + 2u_1 W\cos(\psi - \psi_w) \\ \chi &= \arctan\left(\frac{\dot{y}}{\dot{x}}\right) = \arctan\left(\frac{u_1\sin\psi + W\sin\psi_w}{u_1\cos\psi + W\cos\psi_w}\right) \\ k_\chi(\psi) &= \frac{u_1^2 + u_1 W\cos(\psi - \psi_w)}{V^2} \end{aligned} \tag{4}$$

Note that in the absence of wind (i.e., $W = 0$), $V = u_1$, $\chi = \psi$, and $k_\chi(\psi) = 1$.

The kinematic model given by Eq. (2) essentially assumes the aircraft always makes a coordinated turn and that a fast inner-loop control law is able to achieve the required bank (roll) angle. Thus this model neglects roll inertia. By comparison, the guidance layer model used in [17] uses Eq. (3) based on the assumption that the speed V is known from global positioning system (GPS) measurements and the low-level autopilot provides course angle rate $\dot{\chi} = \alpha_\chi(\chi - \chi_{\text{com}})$ where χ_{com} is the commanded course angle. Because the wind speed appears in the bottom line of Eq. (3) and is unknown, [17] explicitly assumes a high-gain inner-loop controller to reject the wind disturbances to course angle. Robustness to wind in that case is because of the work of the inner-loop controller. Although moving targets could also be incorporated in that approach by using relative target heading measurements, this would rely (perhaps even more) on high-gain inner-loop control. Instead, the approach advocated in this paper is to feed forward estimates of wind and target motion, enabling lower gain in the guidance loop control, which may have robustness advantages in some applications. A hybrid approach is also possible, in which the guidance layer control presented in this article is applied to the wind-robust inner-loop model of [17] to enable tracking of moving targets.

When expressed relative to a target $\mathbf{p}_t = [x_t, y_t]^T$ moving with constant velocity $[\dot{x}_t, \dot{y}_t]^T \in \Re^2$, the aircraft kinematic model Eq. (1) becomes (see Fig. 2)

$$\dot{x}_r = u_1\cdot\cos\psi + W_x - \dot{x}_t \qquad \dot{y}_r = u_1\cdot\sin\psi + W_y - \dot{y}_t \qquad \dot{\psi} = u_2 \tag{5}$$

where $[x_r, y_r]^T = [x - x_t, y - y_t]^T$ is the position of the UA in the target frame. Because the wind velocity and moving target velocity enter Eq. (5) in the same way, it is convenient to consider a single velocity term $[T_x, T_y]^T = [\dot{x}_t - W_x, \dot{y}_t - W_y]^T$. Because the remaining discussion in this paper focuses on the relative motion between the target and the aircraft, we will refer to the *moving target velocity* with the understanding that it is the apparent target velocity that comes from the moving ground target and/or the background wind.

Motion of the aircraft relative to the target, Eq. (5), can also be rewritten in terms of the relative velocity V_r and the relative course angle η

$$\dot{x}_r = V_r\cos\eta \qquad \dot{y}_r = V_r\sin\eta \qquad \dot{\eta} = k_\eta(\psi)\dot{\psi} = k_\eta(\psi)u_2 \tag{6}$$

where if u_1, T_x, and T_y are constant:

$$\begin{aligned} V_r^2 &= u_1^2 + T_x^2 + T_y^2 - 2u_1(T_x\cos\psi + T_y\sin\psi) \\ \eta &= \arctan\left(\frac{\dot{y}_r}{\dot{x}_r}\right) = \arctan\left(\frac{u_1\sin\psi - T_y}{u_1\cos\psi - T_x}\right) \\ k_\eta(\psi) &= \frac{u_1^2 - u_1(T_x\cos\psi + T_y\sin\psi)}{V_r^2} \end{aligned} \tag{7}$$

III. Cooperative Stand-Off Tracking

A. Stationary Loiter Circles

Using the kinematic system model, the SLOS controller generates command inputs for the low-level flight control system based on a Lyapunov vector field approach in which the unmanned vehicle circles about a designated ground target position $[x_t, y_t]^T$. For the moment, the ground target is not moving, and there is no wind. The control maneuvers occur at a commanded altitude h_o with a commanded nominal air speed $u_1 = v_0$ and stand-off radius r_d. The motion is controlled using a Lyapunov vector field first given in [16] to calculate the desired horizontal inertial velocity $[\dot{x}_d, \dot{y}_d]^T$. Then proportional feedback with a feed-forward term is used from the heading angle error to command the turning rate to track the desired velocity.

Consider the Lyapunov function $V(x, y) = (r^2 - r_d^2)^2$, where $r = \sqrt{(x - x_t)^2 + (y - y_t)^2} = \sqrt{x_r^2 + y_r^2}$ is the radial distance of the UA from the ground target position. The total time derivative of $V(x, y)$ is given by $\dot{V} = \nabla V\cdot[\dot{x}, \dot{y}]^T$ and this can be specified to be nonpositive by choosing desired relative velocity $\dot{x}_r = \dot{x}_d$ and $\dot{y}_r = \dot{y}_d$ according to the guidance vector field $\mathbf{f}(x_r, y_r)$ given by

$$\mathbf{f}(x_r, y_r) = \begin{bmatrix}\dot{x}_d \\ \dot{y}_d\end{bmatrix} = \alpha\left(\frac{-v_0}{r}\right)\cdot\begin{bmatrix} x_r\cdot\frac{r^2 - r_d^2}{r^2 + r_d^2} + y_r\cdot\frac{2rr_d}{r^2 + r_d^2} \\ y_r\cdot\frac{r^2 - r_d^2}{r^2 + r_d^2} - x_r\cdot\frac{2rr_d}{r^2 + r_d^2}\end{bmatrix} \tag{8}$$

where α and v_0 are positive. It can be shown that the desired relative speed at any point in this vector field is given by $|f(x_r, y_r)| = \alpha v_0$, except at $r = 0$, in which the vector field is undefined. In polar coordinates this vector field has the form

$$g(r, \theta) = \begin{bmatrix} v_r \\ v_\theta\end{bmatrix}_{\text{des}} = \begin{bmatrix}\dot{r} \\ r\dot{\theta}\end{bmatrix}_{\text{des}} = \alpha v_0\cdot\begin{bmatrix} -\frac{r^2 - r_d^2}{r^2 + r_d^2} \\ \frac{2rr_d}{r^2 + r_d^2}\end{bmatrix} \tag{9}$$

This vector field produces a rate of change of V

$$\frac{dV}{dt} = \frac{-4\alpha v_o r(r^2 - r_d^2)^2}{r^2 + r_d^2} \tag{10}$$

If αv_0 is a function of r, which is bounded away from zero, then the vector field Eq. (8) is autonomous, and by the LaSalle invariance principle [27], r converges to the largest invariant set that makes $\dot{V}$ zero. It can be seen by substituting $r = r_d$ into Eq. (8) or Eq. (9) that the vector field motion on the loiter circle produces $\dot{V} = 0$ and is an invariant solution of Eq. (8). The only other possibility for $\dot{V} = 0$ occurs when $r = 0$. This is excluded by requiring that $r \neq 0$ initially. Then it can be seen that the vector field exits a ball about $r = 0$ containing the initial $r \neq 0$. Hence $r = 0$ cannot be an asymptotic solution. Thus, the vector field is essentially globally asymptotically stable to the loiter circle (i.e., for all initial conditions except $r = 0$). When r is large compared with r_d, the vector field points to the loiter circle center, but the field veers away when approaching the circle to smoothly entrain the motion into a left turn loiter (see Fig. 3a). A right turn loiter can be produced by a sign change in the second terms in Eq. (8), or by a sign change in the second element of Eq. (9).

Feasibility of the desired velocity can be determined by comparing the resulting aircraft heading rates to the maximum value given in Eq. (2). The desired heading ψ_d is calculated from Eq. (8) via

$$\psi_d = \arctan\left(\frac{\dot{y}_d}{\dot{x}_d}\right) = \arctan\left(\frac{y\cdot(r^2 - r_d^2) - x\cdot 2rr_d}{x\cdot(r^2 - r_d^2) + y\cdot 2rr_d}\right) \tag{11}$$

Taking the derivative of Eq. (11) yields

$$\dot{\psi}_d = 4\alpha v_0\frac{r_d r^2}{(r^2 + r_d^2)^2} \tag{12}$$

Equation (12) shows that for $r > r_d$ (i.e., outside the desired loiter circle), the desired turn rate increases monotonically as the radial distance approaches the desired stand-off radius. Thus, for initial

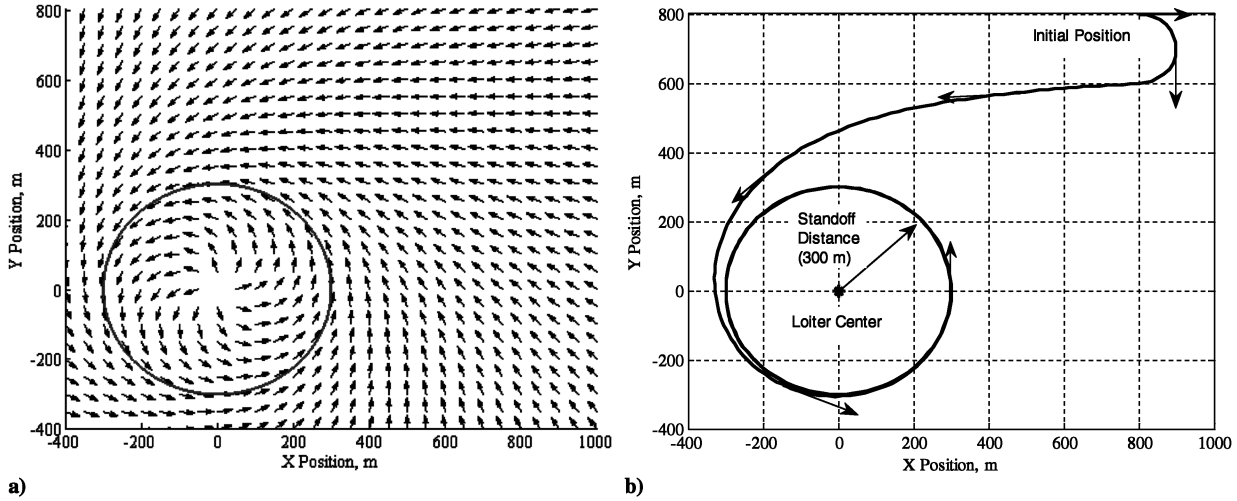

Fig. 3 Example loiter maneuver. a) Lyapunov vector field for loiter maneuver around the origin with a radius of 300 m (solid line). b) The UA begins at (800,800) m and is commanded to loiter around the origin with a radius of 300 m and a speed of 20 m/s.

conditions outside of the loiter circle and $0 < \alpha \leq 1$, trajectories resulting from the guidance vector field Eq. (8) will be feasible as long as the loiter circle pattern itself is feasible, which occurs for $r_d \geq v_0/\omega_{\max}$.

The guidance vector field is used to develop guidance commands for the flight control layer as follows. Equation (1) holds in this case, and u_1 is set to the desired air speed v_o. This is equivalent to setting the scaling factor $\alpha = 1$ in Eq. (8) to produce a constant desired speed along the vector field. Because $\alpha > 0$, this does not affect global convergence of the vector field. The desired heading ψ_d and heading rate $\dot{\psi}_d$ are calculated from Eqs. (11) and (12). The wrapped heading angle error $\langle \psi - \psi_d \rangle$ (such that $-\pi < \langle \psi - \psi_d \rangle \leq \pi$) is multiplied by a gain and added to a feedforward of the vector field turning rate to yield the turn rate command

$$u_2 = -K\langle \psi - \psi_d \rangle + \dot{\psi}_d \tag{13}$$

It is straightforward to see that if $e_\psi = \psi - \psi_d$ then Eq. (13) in Eq. (5) produces $\dot{e}_\psi = -K\langle e_\psi \rangle$, and the heading angle converges exponentially to the desired value with a Lyapunov function $V_\psi = e_\psi^2$, $\dot{V}_\psi = -2Ke_\psi\langle e_\psi \rangle$. On the domain $\Omega = \{ e_\psi : e_\psi^2 \leq m < \pi^2 \}$, $\dot{V}_\psi \leq 0$, hence Ω is positively invariant. On this domain, $\dot{V}_\psi = -2Ke_\psi\langle e_\psi \rangle = -2KV_\psi$ and V_ψ converge exponentially to zero. Because the vehicle speed is set to track the (constant in this case) vector field speed, the vehicle velocity converges to the vector field. Because the vector field is essentially globally stable to the loiter circle, and so is the vehicle [28]. In practice, $r = 0$ is avoided by maintaining the previous guidance vector at any time step where r lies within a specified (small) distance of $r = 0$, which caries the vehicle through this neighborhood in which the vector field varies rapidly.

By assuming that the desired loiter pattern requires a turn rate that is less than the maximum given in Eq. (2), the gain value K in Eq. (13) can be chosen so that the aircraft turn rate constraint is not violated if the aircraft starts outside the loiter pattern. In particular, let the turn rate required to stay on the loiter circle $\dot{\psi}_{\text{circ}} = \dot{\psi}_d(r = r_{\text{des}})$ have magnitude less than the maximum allowable turn rate (i.e., let $|\dot{\psi}_{\text{circ}}| = \omega_{\max} - \varepsilon_\omega$ where $0 < \varepsilon_\omega < \omega_{\max}$). The magnitude of the turn rate command from Eq. (13) is then $|u_2| = |-K\langle \psi - \psi_d \rangle + \dot{\psi}_d|$. From Eq. (12), we have that $|\dot{\psi}_d| \leq |\dot{\psi}_{\text{circ}}|$ for $r \geq r_d$. Because the magnitude of the wrapped heading angle error is always less than π, we can show that $|u_2| \leq K \cdot \pi + \omega_{\max} - \varepsilon_\omega$ for $r \geq r_d$. Finally, to guarantee that $|u_2| \leq \omega_{\max}$, we want $K \cdot \pi + \omega_{\max} - \varepsilon_\omega \leq \omega_{\max}$, which holds for $K \leq K_{\max} = \varepsilon_\omega/\pi$. It should be noted that selection of a gain value greater than $K_{\max}$ does not imply that the tracking controller does not converge to the vector field. In that case, additional analysis is required to consider the control saturation that would be introduced.

Figure 3 shows an example of a UA loitering about a stationary target with constant speed and altitude commands. The UA begins at position (800, 800) m and is commanded to loiter around the target at the origin with a speed of 20 m/s at a stand-off radius of 300 m. The controller uses a turning rate gain value $K = 1.0$.

B. Constant-Velocity Target

Stand-off target tracking of a moving target in the presence of background wind is accomplished using the Lyapunov vector field approach developed in the previous section. The position of the target can be obtained by direct communication with a "friendly" ground vehicle or by estimating it from onboard sensor tracking data. Background wind can be estimated from deviations in the flight path [29] or from air data sensors. If the velocity of the target and background wind are known, a correction term is added as shown next.

If unknown, the constant velocity of the ground vehicle and the background wind velocity act as disturbances to the tracking controller [2], and the basic Lyapunov control scheme described before cannot guarantee that the UA will remain outside of the commanded stand-off distance. To see this, consider the polar coordinate system (r, θ) centered on the inertial target position $\mathbf{p}_t = [x_t, y_t]^T$. Without loss of generality, we can assume the target velocity $\boldsymbol{T}$ is in the inertial x direction and calculate

$$\begin{aligned} \dot{r} &= \dot{x}_r \cdot \cos\theta + \dot{y}_r \cdot \sin\theta = \dot{x} \cdot \cos\theta + \dot{y} \cdot \sin\theta - T_x \cos\theta \\ r \cdot \dot{\theta} &= -\dot{x}_r \cdot \sin\theta + \dot{y}_r \cdot \cos\theta = -\dot{x} \cdot \sin\theta + \dot{y} \cdot \cos\theta + T_x \sin\theta \end{aligned} \tag{14}$$

If the guidance vector field is calculated as if the target is stationary, then the desired inertial velocity would equal the desired relative velocity, which would equal the vector field of Eq. (8) [i.e., $(\dot{x}, \dot{y}) = (\dot{x}_d, \dot{y}_d)$]. Substituting this relationship into Eq. (14) and recognizing that the first two terms on the right hand side become the vector field in polar coordinates from Eq. (9) yields

$$\dot{r} = -\alpha v_0 \frac{r^2 - r_d^2}{r^2 + r_d^2} - T_x \cos\theta \qquad r \cdot \dot{\theta} = \alpha v_0 \frac{2rr_d}{r^2 + r_d^2} + T_x \sin\theta \tag{15}$$

It is easy to see from Eq. (15) that the desired loiter circle is no longer an invariant set. Substituting $r = r_d$ in Eq. (15) yields

$$\dot{r} = -T_x \cdot \cos\theta \tag{16}$$

This expression is only identically zero when $T_x = 0$; otherwise, the vector field has a nonzero radial component at the stand-off

radius. Solving Eq. (15) for the resulting loiter pattern is challenging. However, radial bounds on this new limit cycle can be calculated. In the following, we assume that the target speed does not exceed the desired vector field speed (i.e., $T_x/\alpha v_0 < 1$).

Consider an annulus centered at the target position with inner radius

$$r_{\text{inner}}^2 = \frac{1-\gamma}{1+\gamma} \cdot r_d^2 \tag{17}$$

and outer radius

$$r_{\text{outer}}^2 = \frac{1+\gamma}{1-\gamma} \cdot r_d^2 \tag{18}$$

where $\gamma \in [0, 1)$. Substituting Eq. (17) into Eq. (15) gives the radial component of the vector field on the inner radius of the annulus:

$$\dot{r} = -\alpha v_0 \frac{\frac{1-\gamma}{1+\gamma} r_d^2 - r_d^2}{\frac{1-\gamma}{1+\gamma} r_d^2 + r_d^2} - T_x \cos\theta \;=\; \alpha v_0 \gamma - T_x \cos\theta \tag{19}$$

Note that $\dot{r} \geq 0 \forall\ \theta$ when the inner boundary of the annulus is given in Eq. (17) by $1 > \gamma \geq T_x/\alpha v_0$, and so all trajectories eventually exit the region $r^2 \in (0, \frac{1-T_x/\alpha v_0}{1+T_x/\alpha v_0} \cdot r_d^2)$. Likewise, on the outer radius of the annulus the radial component of the vector field is

$$\dot{r} = -\alpha v_0 \gamma - \ T_x \cos\theta \tag{20}$$

and $\dot{r} \geq 0 \forall\ \theta$ when the outer boundary of the annulus is given in (18) by $1 > \gamma \geq T_x/\alpha v_0$. So all trajectories eventually exit the region $r^2 \in (\frac{1-T_x/\alpha v_0}{1+T_x/\alpha v_0} \cdot r_d^2, \infty)$. Thus, all trajectories are eventually trapped inside an annulus containing the desired loiter circle given by

$$\sqrt{\frac{\alpha v_0 - T_x}{\alpha v_0 + T_x}} \cdot r_d \leq r \leq \sqrt{\frac{\alpha v_0 + T_x}{\alpha v_0 - T_x}} \cdot r_d \tag{21}$$

Furthermore, we know from the Poincare–Bendixson theorem [27] that this region contains a periodic orbit. This result shows that the loiter circle is robust to uncertain wind and target velocity (e.g., T_x) in the sense that small errors relative to the vector field velocity αv_0 produce correspondingly small path tracking errors and that given bounds on the target velocity, the commanded radius can be chosen to ensure that the loiter pattern remains outside the desired radius.

Figure 4 depicts an example of the vector field behavior when the velocity of the target is not known. The UA is commanded to follow and loiter about a target vehicle moving with a velocity of (0, 10) m/s. The UA attempts to maintain a 300 m stand-off distance while traveling at an inertial speed of 20 m/s. Figure 4a shows the path of the UA in an inertial coordinate system, whereas Fig. 4b shows the path of the UA relative to the moving target. The dashed circle in Fig. 4b indicates the stand-off radius of 300 m and the dash-dot lines indicate the bounding annulus defined by Eq. (21). This plot shows the loiter pattern of the aircraft shifted downward relative to the origin (the location of the target) because the target is moving upward in the positive y direction. The UA violates the stand-off distance as it passes in front of the target, which is moving toward it at that time, but stays within the bounding annulus. Figure 4b also shows that the bounding annulus is conservative in the sense that the minimum (maximum) distance that the UA achieves is greater than (less than) the inner (outer) radius of the annulus. A similar result is obtained when wind is present. The vector field is again used as the wind-relative command, which achieves the desired air speed, but the stand-off distance is violated.

When the target and wind velocities are known, a correction term can be added to the desired relative velocity vector, which ensures that the UA remains outside of the stand-off radius. In this case, note that the Lyapunov function given earlier can be considered to be only a function of relative position (x_r, y_r), then the total time derivative of V is given by $\nabla_{x_r} V \cdot [\dot{x}_r, \dot{y}_r]$. Setting $\dot{x}_r = \dot{x}_d$ and $\dot{y}_r = \dot{y}_d$ as given by Eq. (8) produces global convergence to the loiter circle. Using this vector field directly in Eq. (5) produces commands with offsets that depend on wind and target velocity: $u_1 \cos(\psi) = \dot{x}_d - W_x + \dot{x}_t$ and $u_1 \sin(\psi) = \dot{y}_d - W_y + \dot{y}_t$. Unfortunately, this produces an airspeed command that no longer equals a constant speed v_0. We take advantage of the variable scaling factor α in the Lyapunov vector field to change the speed αv_0 of the *relative* vector field to recover a constant air speed v_0 and retain global loiter circle convergence as follows. Set the desired velocity u_1 of the UA to satisfy

$$\begin{bmatrix} u_1 \cos\psi \\ u_1 \sin\psi \end{bmatrix} = \begin{bmatrix} \alpha \cdot \dot{x}_d - W_x + \dot{x}_t \\ \alpha \cdot \dot{y}_d - W_y + \dot{y}_t \end{bmatrix} = \begin{bmatrix} \alpha \cdot \dot{x}_d + T_x \\ \alpha \cdot \dot{y}_d + T_y \end{bmatrix} \tag{22}$$

where T_x and T_y are the (constant) target velocities defined in Sec. II. Taking the norm of Eq. (22) and setting it to the commanded air speed v_o leads to the following expression for the scale factor:

$$\alpha^2 \cdot (\dot{x}_d^2 + \dot{y}_d^2) + \alpha \cdot 2 \cdot (\dot{x}_d \cdot T_x + \dot{y}_d \cdot T_y) + (T_x^2 + T_y^2) - v_0^2 = 0 \tag{23}$$

Provided the UA speed v_o is larger than the target speed, Eq. (23) has one real solution for α, which is positive and bounded away from zero, and only a function of the relative position vector r and the constants T_x, T_y, and v_o. Equation (10) shows that the scaled vector field remains globally convergent to the loiter circle. This value of α

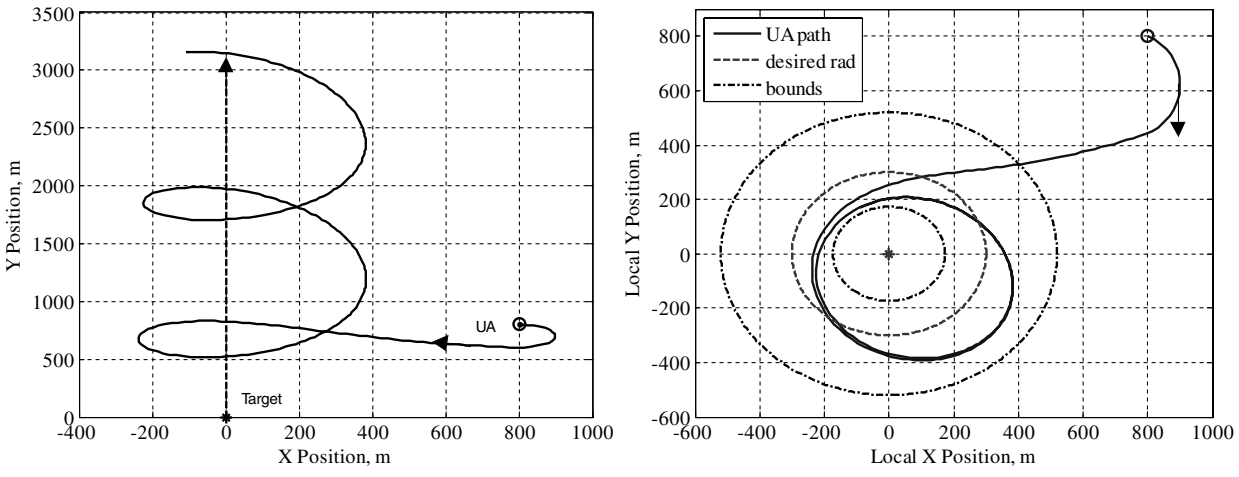

a) b)

Fig. 4 Tracking a moving target without velocity correction. a) The UA begins at (800,800) m and is commanded to follow a target vehicle starting at the origin with a velocity of (0, 10) m/s. The UA is commanded to maintain a stand-off radius of 300 m and a speed of 20 m/s. b) Position of UA relative to the target vehicle. The dashed line indicates the desired stand-off radius. The dot-dash lines indicate the boundary of the trapping annulus given by Eq. (21).

is then used in Eq. (22) to solve for the desired heading angle $\psi_d = \arctan[(\alpha\dot{y}_d + T_y)/(\alpha\dot{x}_d + T_x)]$ or desired relative course angle $\eta_d = \arctan[\dot{y}_d/\dot{x}_d]$.

Similar to the stationary target case, we use a reference tracking control law to regulate the aircraft onto the guidance vector field, which in turn brings the UA onto the desired loiter pattern. Typical sensors onboard small unmanned aircraft can provide inertial velocity $(\dot{x}, \dot{y})$ (e.g., from GPS). Because we also assume the target velocity is known, we can use the (now known) relative velocities $\dot{x}_r = \dot{x} - \dot{x}_t$ and $\dot{y}_r = \dot{y} - \dot{y}_t$ to calculate the relative course angle η from Eq. (6) and compare it to the desired relative course angle. Thus, we use the following reference tracking control law:

$$u_2 = -K(\eta - \eta_d) + \frac{\dot{\eta}_d}{k_\eta(\psi)} \tag{24}$$

where $\dot{\eta}_d$ can be calculated from the expression for desired relative course angle, and $k_\eta(\psi)$ comes from Eq. (7). Stability of this new control law is proven by considering the error $e_\eta = (\eta - \eta_d)$. Taking its derivative and substituting the third line of Eq. (7) yields

$$\dot{e}_\eta = \dot{\eta} - \dot{\eta}_d = k_\eta(\psi)u_2 - \dot{\eta}_d \tag{25}$$

Next, substituting Eq. (24) into Eq. (25) gives

$$\dot{e}_\eta = -K \cdot k_\eta(\psi) \cdot (\eta - \eta_d) + \cdot k_\eta(\psi) \cdot \frac{\dot{\eta}_d}{k_\eta(\psi)} - \dot{\eta}_d \tag{26}$$

which simplifies to

$$\dot{e}_\eta = -K \cdot k_\eta(\psi) \cdot e_\eta \tag{27}$$

When $T_x^2 + T_y^2 < u_1^2$, $k_\eta(\psi) > 0.5 \ \forall \ \psi$ so if $K > 0$, then $K \cdot k_\eta(\psi) > 0.5K > 0$ and

$$\dot{e}_\eta = -K \cdot k_\eta(\psi) \cdot e_\eta < -0.5K \cdot e_\eta \tag{28}$$

and by the comparison principle [27] the relative course error rate has exponential convergence to zero.

An example task when the target velocity is unknown is illustrated in Fig. 5a. The UA is commanded to follow a ground vehicle moving with a velocity of (0, 10) m/s. The UA attempts to maintain a 300 m stand-off distance while traveling at a speed of 20 m/s. Figure 5b shows the results of the same scenario mentioned previously while including the target's velocity.

Although developed to track constant-velocity targets, the modified guidance vector approach can also be applied to some accelerating targets. Figure 6 shows a UA tracking a target moving counterclockwise around a circle of radius $r = 900$ m with a speed of 10 m/s. The path of the target and UA in a global reference frame is given in Fig. 6a, whereas the path of the UA relative to the target is given in Fig. 6b. In this example, the acceleration is slow enough that the desired path remains feasible (i.e., the turn rate constraint is never violated), and so the UA converges to the desired stand-off radius.

C. Coordinated Stand-Off Tracking by Two Vehicles

When a team of vehicles is assigned to follow a single target, coordination between UA is necessary to avoid collisions and to maximize sensor coverage of target vehicle motion. Team tracking can improve sensor coverage when the target vehicle is uncooperative, or is highly agile, such that estimates of its position and velocity are poor. The idea is to distribute UA in the group uniformly in phase on the tracking loiter circle so that unpredicted changes in vehicle motion can be observed and followed at least by the UA in the most advantageous position.

Phase coordination is produced by a second guidance law, which adjusts the speed of the vehicles (within limits) to maintain desired relative phase on the loiter circle provided by the first Lyapunov law Eq. (8). The resulting speed commands are then processed through the correction algorithm Eq. (23) to maintain the desired stand-off distance to the moving target.

Figure 7 shows a two-UA tracking team, with corresponding phase angles θ_1 and θ_2 defined relative to the instantaneous tracking loiter circle. Consider the phasing Lyapunov function

$$V_P = (\Delta\theta - \theta_D)^2 \tag{29}$$

where $\Delta\theta$ is the unwrapped difference between phase angles $\theta_2 - \theta_1$. (Because θ_1 and θ_2 are calculated from inverse tangent functions and typically restricted to $-\pi < \theta_i \leq \pi$, the difference $\Delta\theta$ may be discontinuous. *Unwrapping* maintains continuity of the difference $\Delta\theta$ by adding/subtracting 2π from $\Delta\theta$ if it changes by more than $\pm\pi$ over one sample period.) The time rate of change of the phasing Lyapunov function is

$$\frac{d}{dt}V_P = 2(\Delta\theta - \theta_D)(\dot{\theta}_2 - \dot{\theta}_1) \tag{30}$$

Choosing the angular speed commands

$$\dot{\theta}_1 = k \cdot \left(\frac{r_d}{r_1}\right)^2 \cdot \langle \Delta\theta - \theta_D \rangle + v_0/r_d \tag{31}$$

$$\dot{\theta}_2 = -k \cdot \left(\frac{r_d}{r_2}\right)^2 \cdot \langle \Delta\theta - \theta_D \rangle + v_0/r_d \tag{32}$$

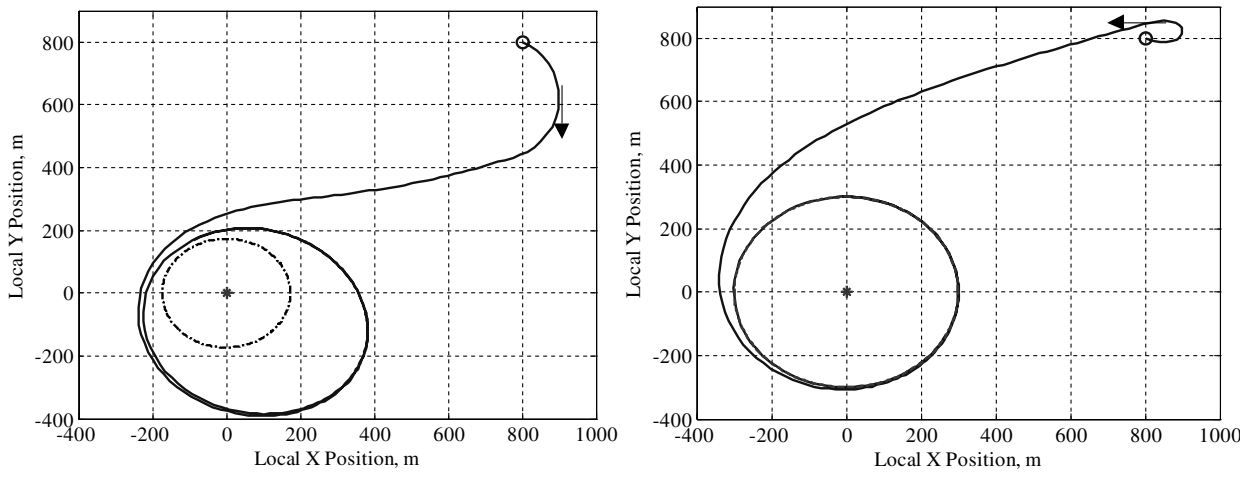

Fig. 5 Position of UA relative to a moving ground target using a) position of GV only, and b) position and velocity of GV. The dashed line indicates the commanded stand-off radius. The UA begins at (800,800) m and is commanded to follow a GV starting at the origin with a velocity of (0, 10) m/s. The UA is commanded to maintain a stand-off radius of 300 m and an air speed of 20 m/s.

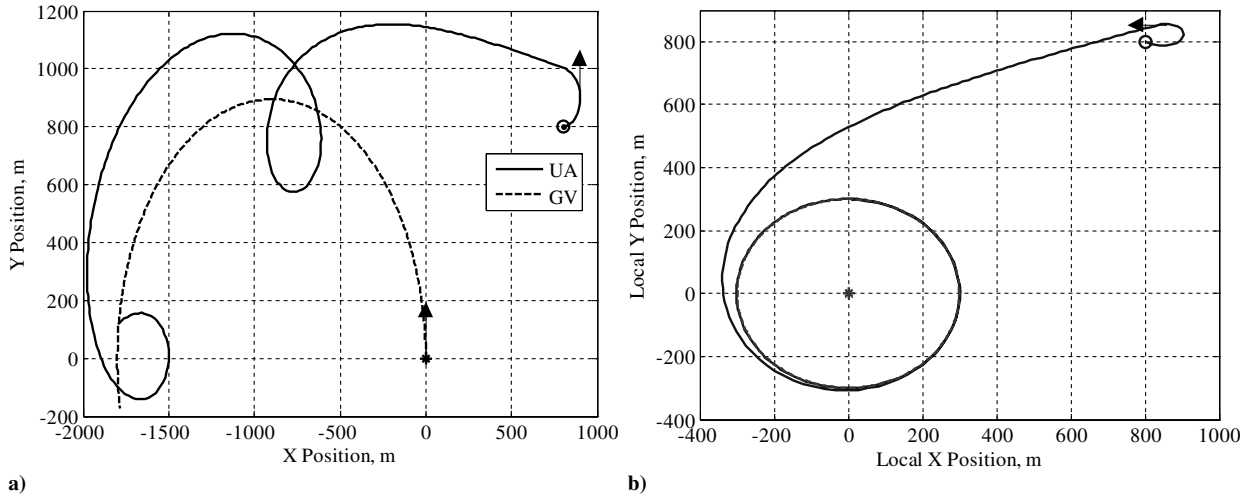

Fig. 6 A UA tracking a surface target moving in a circle. a) The UA begins at (800,800) m and is commanded to follow a surface vehicle starting at the origin with speed 10 m/s. The UA is commanded to maintain a stand-off radius of 300 m and a speed of 20 m/s. b) Position of UA relative to the target vehicle. The dashed red line indicates the desired stand-off radius.

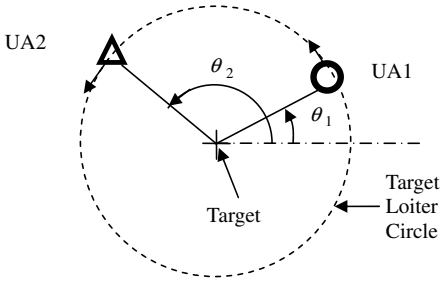

Fig. 7 Phase angles for a team of UA tracking a single target.

where $\langle \Delta\theta - \theta_D \rangle$ is wrapped such that $-\pi < \langle \Delta\theta - \theta_D \rangle \leq \pi$, results in

$$\frac{d}{dt} V_P = -4k \left(\frac{r_d}{r} \right)^2 (\Delta\theta - \theta_D) \langle \Delta\theta - \theta_D \rangle \tag{33}$$

On the domain $\Omega_P = \{ \Delta\theta \colon \Delta\theta - \theta_D \leq m < \pi^2 \}$ (which excludes the case that the angle difference and desired angle differ by π, corresponding to $\theta_2 = \theta_1$ for $\theta_D = \pm\pi$) and $\dot{V}_P \leq 0$, Ω is positively invariant. On this domain, $\dot{V}_P = -4k(\frac{r_d}{r})^2(\Delta\theta - \theta_D)^2 = -4k(\frac{r_d}{r})^2 V_P$, and V_P converges exponentially to zero. Because r is monotone deceasing for each UA (because of the vector field of Eq. (9)) if it is initially larger than the loiter circle, and is monotone increasing if it is initially inside the loiter circle, $(r_d/r)^2 \geq (r_d/r_0)^2 > 0$ is bounded away from zero based on the initial range r_0 of the UA to the target. By the comparison principle [27], V_P converges exponentially to zero; hence, the relative angle $\theta_2 - \theta_1$ converges exponentially to the desired phase offset θ_D. The corresponding speed commands to the flight control subsystems are then

$$\begin{aligned} u_{1,1} &= k \cdot \left(\frac{r_d}{r} \right)^2 \cdot (\theta_2 - \theta_1 - \theta_D) r_d + v_0 \\ u_{1,2} &= -k \cdot \left(\frac{r_d}{r} \right)^2 \cdot (\theta_2 - \theta_1 - \theta_D) r_d + v_0 \end{aligned} \tag{34}$$

The scaling term $(r_d/r)^2$ is used to deemphasize phase separation when the UA are far from the target (i.e., $u_{1,i} \approx v_o$ for $r \gg r_d$).

In the case of a two-UA team, we choose the offset θ_D to be an odd multiple of π radians to mitigate against target maneuvers. Other team objectives, such as optimal geolocalization, would use different phase offsets. It is interesting to note that the multiple of π chosen determines which UA is phased ahead of the other. For example, choosing the odd multiple of π closest to the initial angular offset of the UA preserves their initial ordering in phase on the loiter circle. Choosing a different multiple of π causes one UA to overtake the other, switching the phase order before settling to the desired 180 deg relative offset.

Figure 8 shows the results of the overall control scheme, in which two UA act in a team to follow a moving target, maintaining a desired stand-off distance as well as a desired loiter circle phasing. The left plot shows UA paths in local coordinates, in which the vehicle to be tracked moves with a constant velocity of 10.0 m/s along the y direction. There is no wind in this case. It is clear that the UA are attracted to a loiter circle about the target vehicle, and maintain the desired stand-off distance (300 m). Figures 8b and 8c show the stand-off distance and phase angle separation of the vehicles versus time. The air speeds of the UA were restricted to $v_0 - 5$ m/s $\leq u_{1,i} \leq$

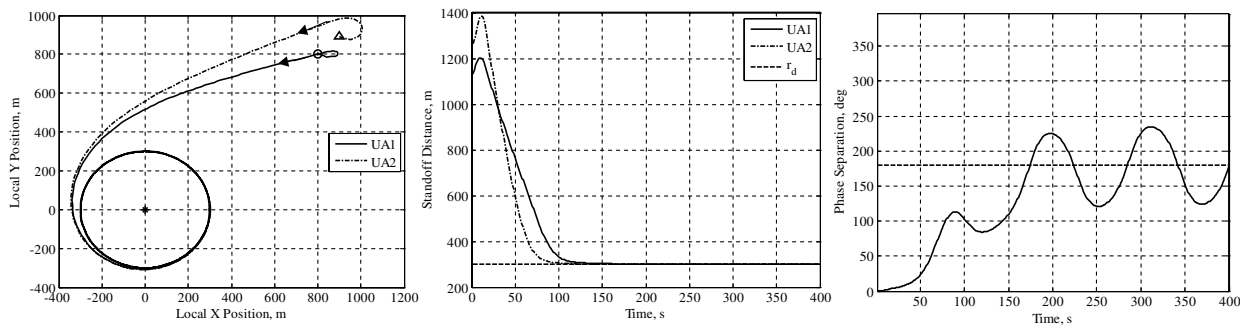

Fig. 8 Two UA tracking a moving target. a) UA positions in local coordinates; b) stand-off distance vs time; c) phase separation vs time.

$v_0 + 5$ m/s with $v_0 = 20$ m/s, and a maximum turn rate $|u_2| \leq 0.2$ rad/s was enforced. The analysis in Eqs. (29–34) assumes a static target and no airspeed constraints. When the target moves, the airspeed required to achieve a given transverse velocity ($\dot{\theta}$) can become exceedingly large. See [2] for more detail on the effect of wind speed (and therefore target speed) on transverse velocity. The airspeed constraints prevent the UA from achieving the transverse velocities specified by Eqs. (31) and (32). Because the effects of the airspeed limitations are not symmetric, they prevent the vehicles from converging to the desired phase spacing. However, the resulting behavior can still produce the desired stand-off distance and reasonable phase separation in tracking a moving target.

D. Convoy Protection

Ground vehicle tracking for convoy protection is achieved by again modifying the Lyapunov controller. In particular, the circular pattern relative to the ground vehicle is lengthened to include two straight-line segments along the direction of travel of the ground vehicle. The new pattern is defined by four parameters, the straight-line distance D_f to cover in front of the ground vehicle, the straight-line distance D_b to cover behind the ground vehicle, the radius R_t of the turn made at either end of the pattern, and the fractional offset f_{off} of the pattern from the ground vehicle center. The pattern relative to the ground vehicle (at the origin, moving in the x direction) is illustrated in Fig. 9.

For convoy protection, the UA controller divides the region around the ground vehicle into four quadrants (Fig. 9) defined by the lines through $\{X_{11}, X_{12}\}$ and $\{X_{21}, X_{22}\}$. In quadrant I, the controller uses the Lyapunov algorithm [Eq. (8)] described before. In quadrant II, the controller aims the UA at point X_{21} to drive the UA toward the desired pattern (as opposed to traveling straight across). Quadrant III returns to the Lyapunov approach (with a different loiter circle center), and in quadrant IV, the controller aims at point X_{22}. Figure 10 shows the guidance vector field for the convoy protection controller. The discontinuities in the vector field are not a problem for the reference tracking controller given by Eq. (24) because $\dot{\psi}_{\text{des}}$ can be calculated numerically.

When two UA are assigned to track a friendly vehicle, Eq. (34) is used to maintain relative phasing and separation. In this case, phase separation still refers to the difference in the azimuthal angular positions of the two aircraft in polar coordinates centered on the target (e.g., $\theta_2 - \theta_1$). Figure 11 shows two UA following a friendly vehicle traveling with a speed of 10 m/s. The parameters used to define the tracking pattern are $D_f = 1000$ m, $D_b = 300$ m, $R_t = 300$ m, and $f_{\text{off}} = 0.5$. Figure 11a shows the paths of the UA in the inertial frame, and Fig. 11a shows the paths of the UA relative to the moving ground vehicle. Figure 11c shows the separation distance between each UA and the ground vehicle, which varies (as expected) between $[R_t, R_t + D_f]$. Figure 11d shows the phase separation between vehicles which are trying to achieve a value of 180 deg (dashed line).

IV. Simulation Results

In this section, we use several different simulation studies to analyze the performance of the cooperative tracking algorithms. In particular, three different case studies are made. First, we look at stand-off tracking of an adversarial target that can detect the position of one of the UA. Performance, in terms of separation distance, is compared between single vehicle tracking and cooperation between two UA. Second, convoy protection is evaluated based on the percentage of time the (friendly) target is in view of at least one UA, and the percentage of time the target is on ground and is not surveyed by any vehicle. Finally, a hierarchical cooperative search, acquisition, and tracking architecture is described that uses the cooperative stand-off tracking algorithms as the middle layer of a hierarchical system. Simulation results using this architecture illustrate how the guidance vector field approach enables simple abstractions at different levels of a hierarchical system that combine to enable complex operation.

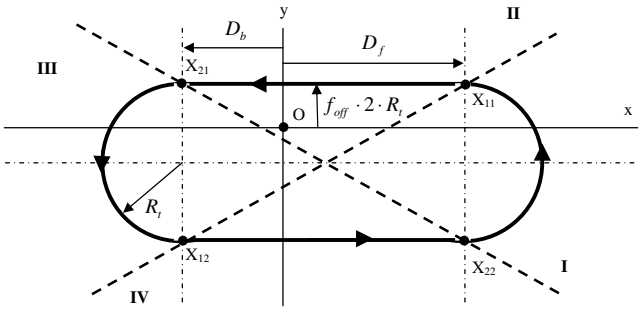

Fig. 9 Tracking pattern of a single UA in convoy protect mode.

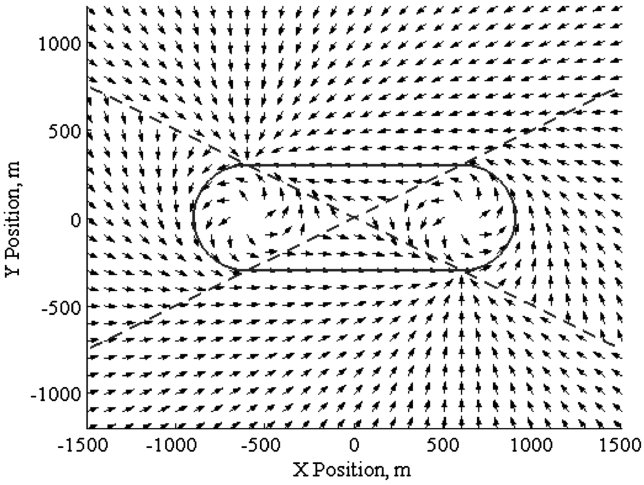

Fig. 10 Guidance vector field for convoy protection. The solid line denotes the desired orbit pattern and the dashed lines indicate the different quadrants.

A. Tracking Adversarial Targets

The value of cooperative phasing by multiple UA depends on the mission scenario, vehicle capabilities, and target response. For geolocalization tasks in which the goal is to determine the position and velocity of a moving target, optimal performance occurs with phase spacing of 90 deg between vehicles [24]. In contrast, maintaining track (i.e., visibility) of an adversarial target requires different spacing and motivates the baseline 180 deg separation used here.

This section presents simulation results to verify the performance increase in terms of minimum stand-off distance between any UA in the team and an evading target. Simulations were run using a maximum turning rate $\omega_{\max} = 0.1$ rad/s, nominal speed $v_0 = 25.0$ m/s, speed constraint $v_0 - 5$ m/s $\leq u_{1,i} \leq v_0 + 5$ m/s, and no background wind. For the single-UA case, the aircraft flies with maximum speed $u_{1,1} = v_0 + \Delta v_{\max} = 30$ m/s. The UA use only the position of the target (and not its velocity) to derive the guidance vectors. The UA begin the simulation at the desired stand-off distance and (for the two-UA case) with the desired phase separation. In these examples, the ground target attempts to evade the UA team by always moving in the direction opposite the relative position vector from the target to the midpoint of the line segment connecting the two UA. That is, the target is attempting to evade both UA at the same time by evading their centroid. Although the gimbal excursion range is a concern for fielded systems, the values in these simulations are always within acceptable limits and are not discussed further. The azimuth (bearing) angle is always between -30 and -180 deg, whereas the elevation angle is a function of UA height but is kept within a small range because the UA always turn (and hence bank) in the same direction.

Figure 12a shows plots of separation distance error (i.e., actual separation minus 300 m desired stand-off distance) versus time between the evader and the UA for both the one-UA and two-UA

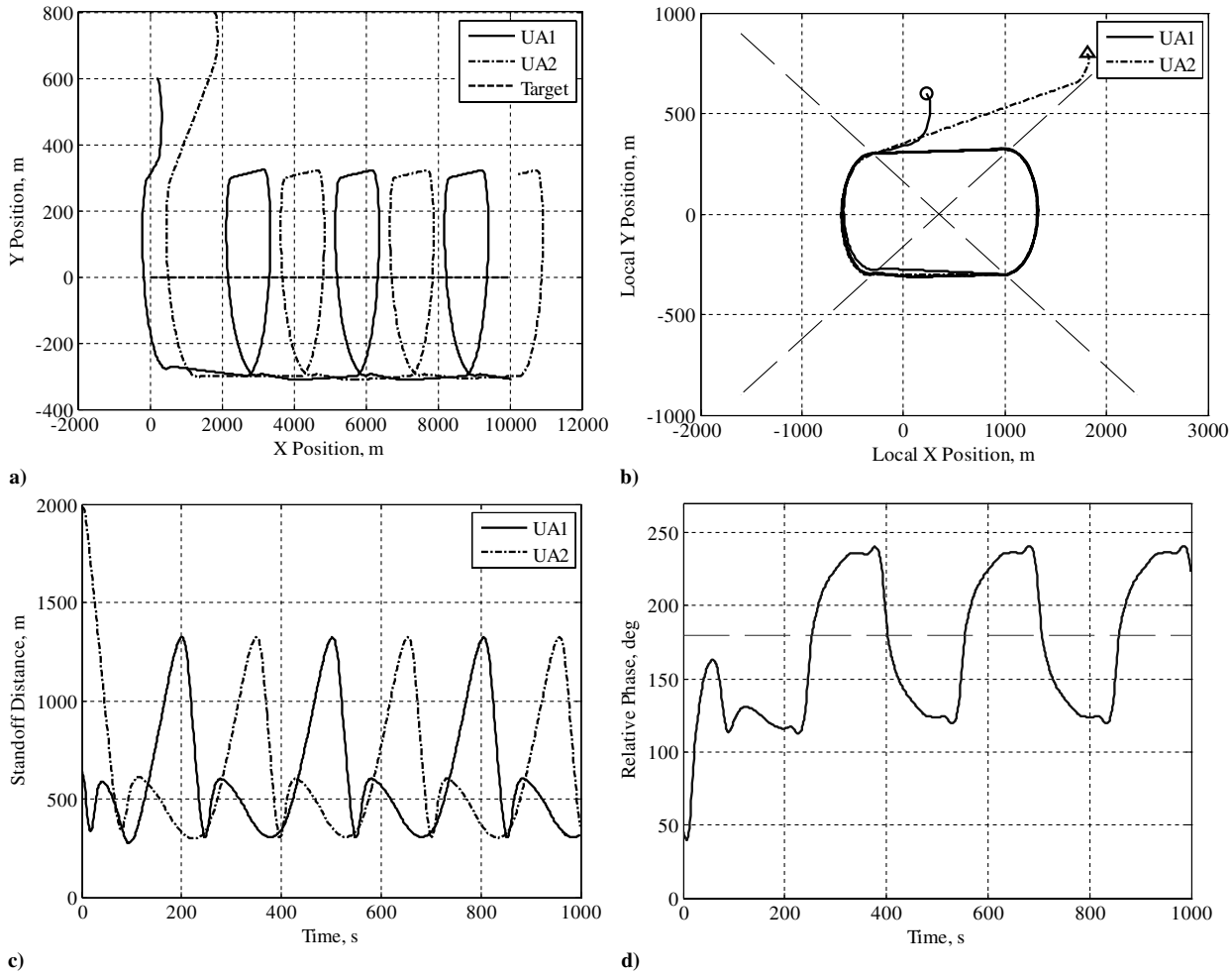

Fig. 11 Two UA performing convoy protection. a) Paths of the UA in the inertial coordinate system; b) paths of the UA in the coordinate system relative to the target vehicle; c) stand-off distances of UA from target; d) phase angle separation between UA.

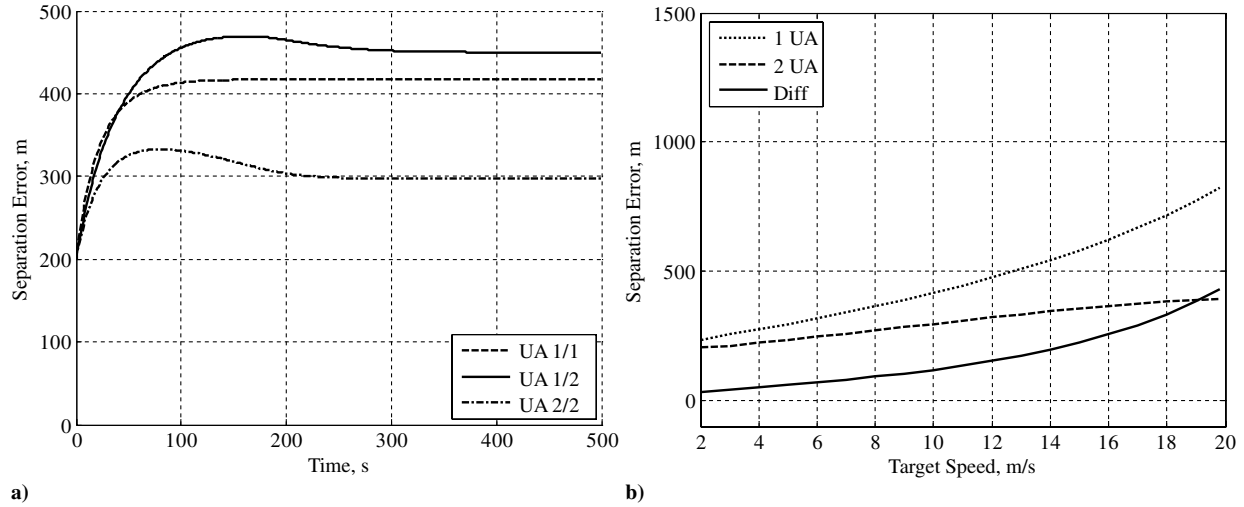

Fig. 12 UA tracking an evading target with nominal UA speed of 25 m/s. a) Separation distance error versus time for case when target speed is 10 m/s. b) Final separation distance error and performance improvement (difference) versus target speed (m/s).

cases with target speed 10.0 m/s. The evader is able to achieve a large steady-state separation because the UA cannot anticipate its evasive maneuver. In this example, the evading target can maintain a separation distance error of approximately 415 m (actual separation of 715 m) from the single UA. When two UA coordinate their actions, the target can only maintain separation error of approximately 300 m from the team. In this case, the presence of the second UA limits the movement of the target, preventing it from moving directly away from either vehicle.

Figure 12b shows tracking performance, in terms of minimum separation distance error from any UA, versus target speed. Also, improvement in performance between the one-UA and two-UA cases is shown by taking the difference of the performance measures for either case. Tracking performance is measured by the steady-state

separation distance error between the target and the UA. For the two-UA case, the minimum of the distances from either UA to the target is used. As expected, Fig. 12b shows that as the target speed increases, it is able to achieve larger separation from the UA team. This increased separation distance corresponds to a decrease in performance because larger separation reduces the resolution of any sensor covering the target. However, performance is improved, and the steady-state separation distance is reduced with the addition of a second UA in the scenario. Improvement in tracking performance (solid line in Fig. 12b) is shown by subtracting the two-UA result from the one-UA case. As already discussed, performance is improved, in terms of less separation, by adding a second UA for all target speeds. Furthermore, this improvement increases as a function of target speed. As the target speed approaches the minimum speed of the UA, the benefit of cooperation increases. In other words, cooperation improves tracking the most for fast moving targets.

B. Convoy Protection

The value of cooperative convoy protection is measured by several different metrics that describe the total UA team sensor coverage. Because the main goal of convoy protection is to prevent ambush or attack by hidden forces, the performance metrics used here focus on total coverage by the sensor team of the area the convoy traverses and not just maintaining the ground vehicle (GV) in the field of view of one sensor at all times. Thus, metrics of interest include the fraction of time the GV is in view of at least one UA sensor, the fraction of time the GV is within the total area swept out thus far by the UA sensors (alternatively, this metric is 1.0 minus the fraction of time the GV is in unexplored territory), and the minimum distance between the GV and the frontier of the unexplored region.

At a given time, a target vehicle is *in view* if it is within the sensor footprint of at least one UA at that time. We refer to the total area swept out by the UA sensors over time as the *coverage area* and the edge of this region as the *coverage boundary*. Thus, a target vehicle that is in view of one or more UA is necessarily in the coverage area; however, a target does not have to be in view to be in the coverage area. By definition, the region of the environment outside of the coverage area has not been visited by any UA sensor and may therefore contain undetected threats.

Simulation experiments were conducted with a single GV moving in a straight line along the positive x direction with speeds that varied from 4.0 up to 20.0 m/s (the nominal speeds of the UA). UA initial positions were determined randomly by adding a random vector to a default initial condition. The first UA began at the origin with random offset in both directions selected uniformly from $-300 \leq p_{\text{offset}} \leq 300$ m, whereas the second UA had a default location of [0.0, $0.8D_f$ m] and selected a random offset from the same uniform distribution. Initial velocities of both UA were in the positive x direction. The aircraft were assumed to fly at a height of 500 m above the ground with a sensor that has a 70 deg field of view, corresponding to a circular sensor footprint with 350 m radius. It is assumed that this footprint includes the field of view of the sensor itself and any gimbal excursion limits (i.e., the sensor sweeps out a circular pattern quickly relative to UA flight speed). Roll motion of the aircraft is not considered when determining the sensor footprint. The parameters used to define the tracking pattern (Fig. 9) are $D_f = 1000$ m, $D_b = 300$ m, $R_t = 300$ m, and $f_{\text{off}} = 0.5$. For each scenario (one or two UA), 20 simulations with randomly selected initial conditions were run for each target speed.

Figure 13 contains results from individual simulation runs for different values of ground target speed. Each plot shows the distance from the target to the coverage boundary as a function of time for the one-UA (dashed line) and two-UA (solid line) scenarios. For a target speed of 4 m/s (upper left plot,) steady-state behavior is similar for both scenarios, and the UA maintain a distance of approximately 650 m between the target and the coverage boundary. For higher target speeds (other subplots), steady-state behavior becomes periodic as the target gets closer and farther from the coverage boundary. The final plot (lower right) shows that the target leaves the coverage area at some times during the run (denoted by a distance of zero to the coverage boundary).

Figure 14 compares several metrics for the one-UA and two-UA cases. The results presented here are averaged over the 20 runs taken for each case at each target speed value. Figure 14a shows the minimum distance from the target to the coverage boundary in steady state (i.e., after approximately 250 s in Fig. 13) for different values of target speed. This minimum distance is always greater for the two-UA case but decreases as the target speed increases. For the single-UA case, the target leaves the coverage area and enters the unexplored region for some portion of time (indicated by the fact that the minimum distance becomes zero) for speeds greater than 10.0 m/s. Likewise, for the two-UA case, the target leaves the coverage area for speeds greater than 12.0 m/s. Figure 14b depicts sensor coverage for different target speeds. Both time in view and time in the coverage area are depicted. For slow speeds (<10.0 m/s) the target remains in the coverage area throughout the entire run. As the speed increases, the fraction of time the target is in the coverage area decreases. For the single-UA case, this fraction decreases to zero when the target has the same speed as the UA. For the two-UA case, the target remains in the coverage area approximately 80% of the time, even for a fast moving target. Compared with the fraction of time the target stays in the coverage area, the fraction of time the target is in view of at least one sensor exhibits unexpected behavior. For the one-UA case, the target stays in view for more time as the target speed increases until the curve bends back towards zero at a target speed of 14.0 m/s. On the other hand, the plot for the two-UA

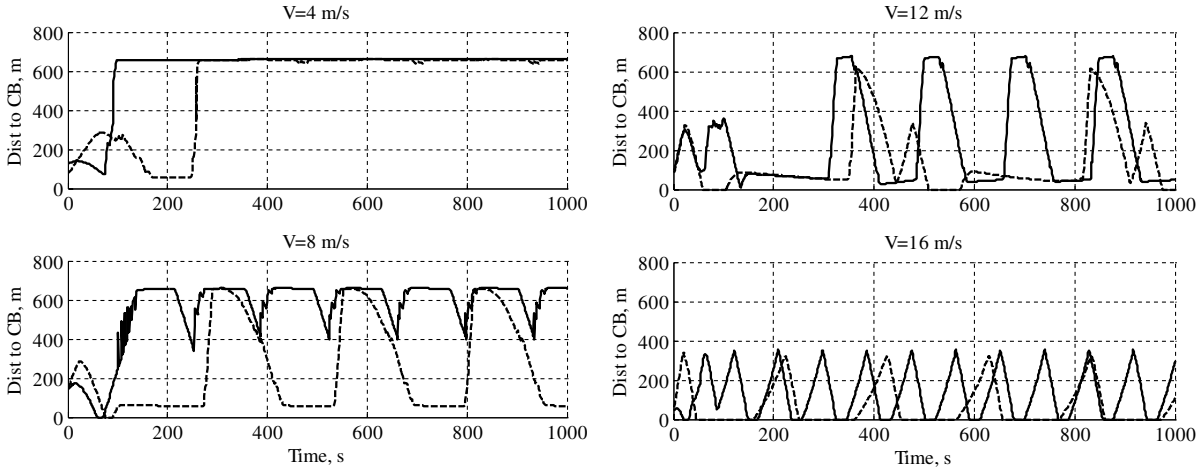

Fig. 13 Example results from convoy protection simulations. For a single simulation run, plots show distance from ground target to coverage boundary versus time for different values of target speed. The dashed lines denote the one-UA case and the solid line denotes the two-UA case.

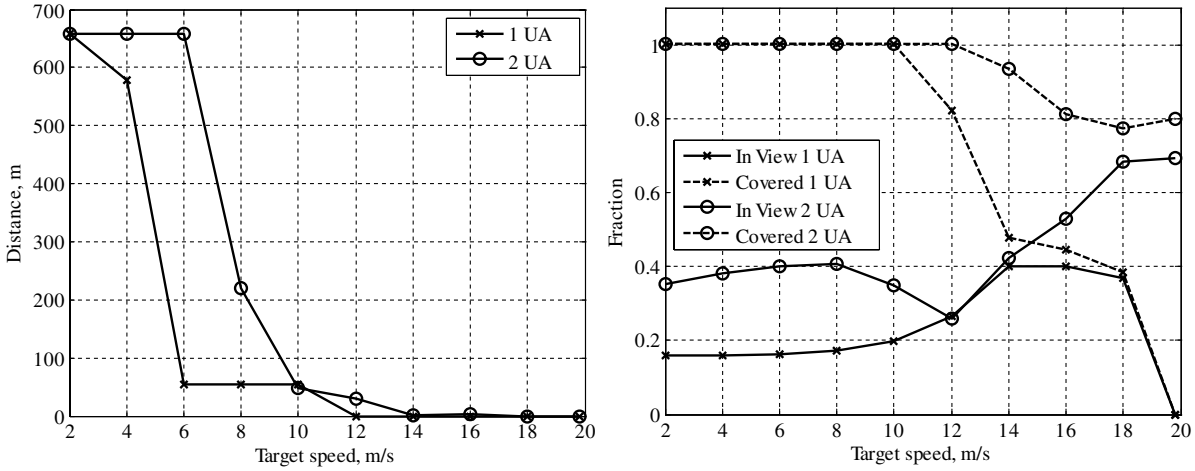

a) b)

Fig. 14 Comparison of convoy protection metrics for single- and two-UA scenarios (nominal UA speed equal to 20 m/s). a) Minimum distance to coverage boundary. b) Fraction of time GV is in view and in the covered area.

case initially rises, begins to drop at a target speed of 6.0 m/s, and then increases again beyond 12.0 m/s. These results are because of the fact that the fraction of time in view is heavily dependent on the initial conditions, and parameter values used in the simulation and for the values presented here demonstrates a distinct bimodal distribution (not shown), which skews the average result. However, the main observation is that cooperation (i.e., adding the second UA), improves both metrics compared with the single-UA scenario.

A final comparison is made using an average threat exposure metric. For point threats, a Gaussian distribution is often used to relate the exposure level to some statistical representation of the threat [30]. In the work presented here, the surveillance by the UA team does not reveal threats, but instead reveals regions that are clear of threats. The entire unsensed region represents a possible threat. Intuitively, exposure to possible threats is greater as the vehicle approaches the unsensed region (which could contain a threat). Thus, we assume exposure to enemy threats α_{exp} is inversely proportional to the square of the distance from the target to the coverage boundary d_{CB}

$$\alpha_{\text{exp}} \propto \frac{1}{(d_{\text{CB}} + \varepsilon)^2} \tag{35}$$

where ε is a small bias that ensures that the exposure metric is defined on or beyond the coverage boundary ($d_{\text{CB}} = 0$). The average exposure is then defined as the summation of threat exposure at each sample time

$$\bar{\alpha}_{\text{exp}}[k_f] = \sum_{k=k_s}^{k_f} \frac{1}{(d_{\text{CB}}[k] + \varepsilon)^2} \tag{36}$$

Figure 15 shows plots of the mean (over the 20 simulation runs) of the average threat exposure versus target speed for each scenario. For each scenario threat, exposure increases as target speed increases, because the target approaches closer to the coverage boundary, even leaving the coverage area at times. Compared with the single-UA case, the addition of a second UA reduces the threat exposure by approximately an order of magnitude at every target speed.

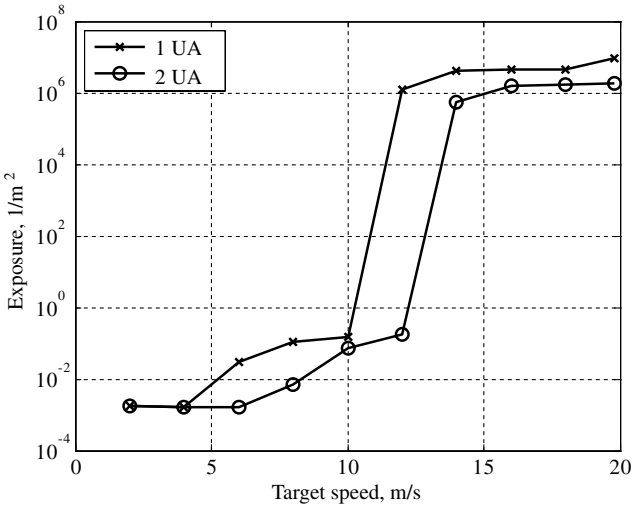

Fig. 15 Semilog plot of average threat exposure versus target speed for one-UA (dashed) and two-UA (solid) scenarios.

C. Cooperative Search, Acquisition, and Tracking

This section illustrates how the cooperative stand-off tracking and convoy protection guidance techniques can be used in a larger cooperative search, acquisition, and tracking (CSAT) architecture (Fig. 16). The CSAT architecture uses a centralized team coordination layer to assign UA to different tasks that include a location or target and a mode of operation. A midlevel guidance layer implements different UA modes based on the SLOS tracking controllers presented in Sec. III. Use of the guidance vector field control at the middle layer enables abstraction of the control mode behavior by the team coordination layer. Because the guidance vector field control is globally stable, the coordination layer can make assignments based on a single metric such as the distance between each target and UA (which is a measure of relative intercept time for stationary targets). Thus, the combination of relatively simple, provably well-behaved algorithm at different levels in a hierarchical control architecture leads to cooperative group behaviors capable of carrying out complex missions. The simulation results show a single example of a mission carried out using the CSAT architecture, highlighting the use of the guidance vector field approach in a hierarchical cooperative control framework.

The midlevel trajectory guidance layer (Fig. 16) is made up of the following modes derived from the SLOS tracking algorithms: LOITER, FOLLOW, PROTECT, SUPPORT, SUPPORT_PROTECT, and SEARCH. The LOITER, FOLLOW, and PROTECT modes are the stationary target, moving target, and convoy SLOS tracking controllers, respectively. The two SUPPORT modes correspond to the second UA in the cooperative versions of the FOLLOW and PROTECT modes and are commanded to higher altitudes to provide wider sensor coverage. The SEARCH mode is a standard lawn mower pattern over a region determined by the team coordination layer.

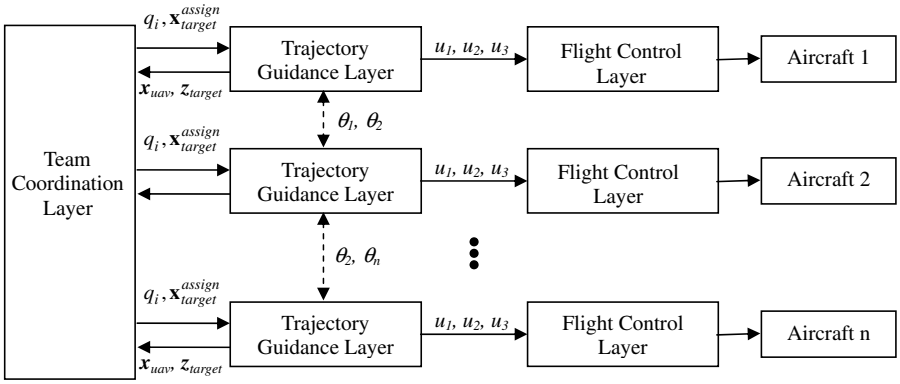

Fig. 16 Cooperative search, acquisition, and tracking architecture.

The coordination layer assigns each UA in the team to different tasks based on the number of targets that have been discovered and the number of UA in the team. The team coordinator has global knowledge of the UA locations and any area they have covered. The coordinator makes assignments in the following priority order: 1) each target vehicle is FOLLOWED by one UA; 2) each UA in FOLLOW mode is SUPPORTED by one UA; 3) remaining UA are assigned to SEARCH. Assignment is performed using binary integer programming to minimize

$$\sum_{i=1}^{n}\sum_{j=1}^{m} t_{ij} \cdot x_{ij} \tag{37}$$

subject to

$$\sum_{i=1}^{n} x_{ij} \le 1 \qquad \sum_{j=1}^{m} x_{ij} = 1 \qquad m \le n \tag{38}$$

or

$$\sum_{i=1}^{n} x_{ij} = 1 \qquad \sum_{j=1}^{m} x_{ij} \le 1 \qquad n \le m \tag{39}$$

$$x_{ij} \in \{0, 1\} \tag{40}$$

where m is the number of targets, n is the number of UA, $t_{ij} = r_{ij}/(v_i - v_j)$ is an estimate of the time needed by UA_i to intercept target_j, r_{ij} is the distance from UA_i to target_j, v is the UA or target speed, and x_{ij} is an assignment variable that is equal to 1 if UA_i is assigned to target_j and zero otherwise.

A scenario is considered that includes six UA, two unclassified/adversarial ground vehicles, and one friendly ground vehicle. Thus, one UA is assigned to FOLLOW/PROTECT each ground vehicle, and one UA SUPPORTS each UA in FOLLOW/PROTECT mode (by tracking the same target vehicle). Initial UA positions are selected randomly. Sensor coverage is modeled by circular footprints on the ground, and terrain obstructions are modeled as regions of zero sensor coverage. Two unviewable regions are included that lie on roads in the simulation environment. These regions have radii of 350 and 400 m. Unclassified targets are only detected if they come within the sensor footprint of a UA, whereas friendly vehicles are detected once they enter the environment. Parameter values for the simulation are given in Table 1.

To discuss the performance of the CSLOS tracking in this CSAT application, we look at the simulation results from the perspective of the different target vehicles, starting with the friendly vehicle that has two UA performing convoy protection overhead. Figure 17a shows the paths of two UA as they track a friendly ground target (dashed line). The discontinuities in the UA paths (most evident on the dark solid path in the center of the figure) are because of target hand off commanded from the coordination layer. Thus, the two curves do not represent paths taken by two specific UA, but rather a concatenation of path segments by the UA assigned to protect the friendly target. The main goal of the PROTECT mode is to provide situational awareness around the region of a moving vehicle or convoy. The flight pattern depicted in Fig. 9 provides elongated orbits in a frame of reference relative to the moving vehicle. Figure 17b shows the distance from the target to the coverage boundary. Once detected (at time t = 272 s), the target remains in the coverage area at all times even though it changes directions at several points. This indicates that the future ground vehicle position is always surveyed before the vehicle arrives, providing advance warning for possible threats.

Tracking of unclassified targets using the CSLOS control described in Sec. III.C is performed on two ground targets by four UA. Figure 18 shows the paths of the two UA tracking the first and second ground vehicles, respectively. During its motion, GV1 enters both zero-visibility regions (shaded disks) causing the UA to loiter until it reappears and tracking resumes. The paths of GV1 and GV2 overlap, causing a target hand off between vehicle teams (see Fig. 19). Thus, like the paths shown in Fig. 17a, the paths in Fig. 18 are concatenations of path segments for the individual UA that tracked the targets throughout the simulation. Figure 18c shows the separation distances between the UA and the targets they are assigned to track. For most of the simulation, the UA remain outside the specified stand-off distance of 200 m (dashed line). The exceptions at t = 300 s and t = 400 s are because of the reassignment described next.

The team coordination layer of the CSAT architecture initiates target hand off between UA based on the estimated target intercept

Table 1 Parameter values for CSAT simulation

Parameter	Value
Simulation environment size	3600 × 4200 m
Nominal speed v_0	20 m/s
Stand-off radius r_d	200 m
Maximum speed increment	5.0 m/s
Maximum turn rate	0.2 rad/s
Sensor field of view	70 deg
Assigned height: SEARCH, LOITER	1000 m
Assigned height: FOLLOW, PROTECT, SUPPORT_PROTECT	500 m
Assigned height: SUPPORT	750 m

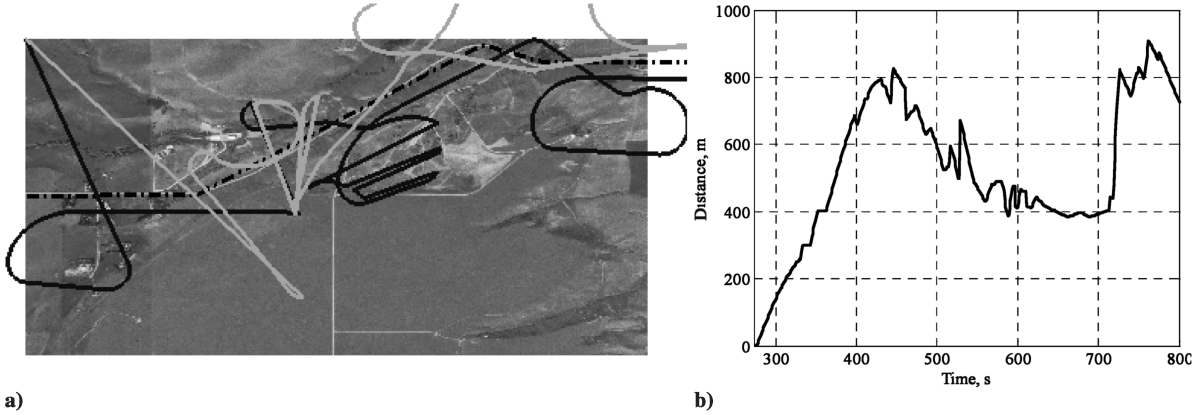

Fig. 17 Convoy protection of a single friendly vehicle by two UA. a) Paths of UA (solid lines) and target (dashed line). b) Distance from target to coverage boundary versus time.

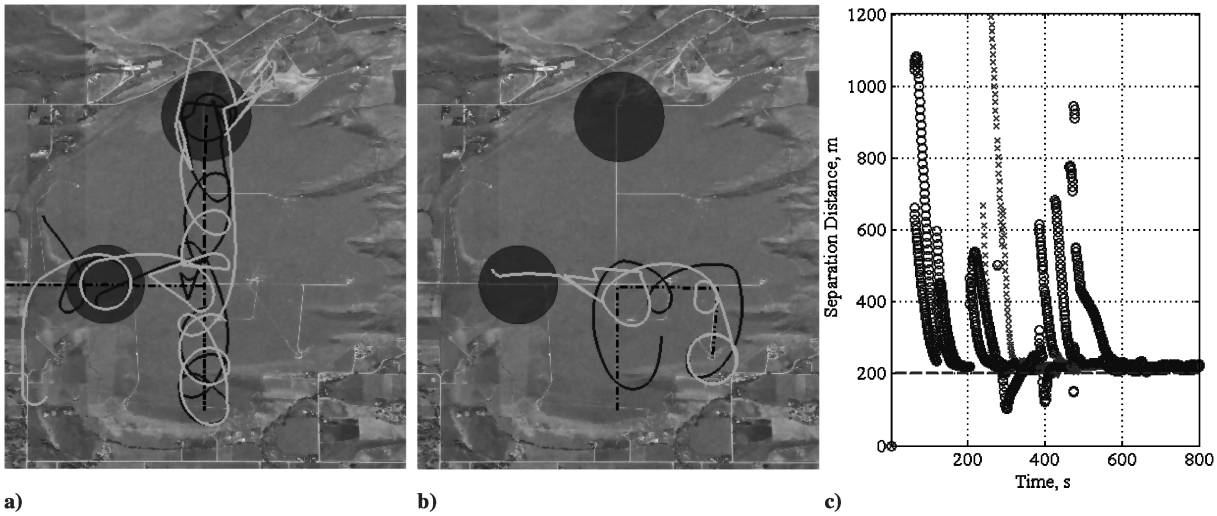

Fig. 18 Paths of the UA tracking unclassified ground targets. a) UA tracking target GV1; b) UA tracking target GV2; c) separation distance between targets and the UA tracking them. Distances to GV1 are marked by the "o" whereas distances to GV2 are marked by the "x."

times. Abstraction of the midlevel guidance layer allows the team coordinator to reassign targets based on a single parameter (the estimated intercept time, based on the value of the guidance Lyapunov function), whereas the global stability property of the guidance vector field provides predictable behavior when UA switch targets. The motion of the ground vehicles brings GV1 and GV2 into close proximity at the intersection in the middle of the simulation environment. This causes a reassignment of UA to different targets based on relative distance. Figure 19 shows a sequence of snapshots during which the hand-off maneuver occurs. At time $t = 270.0$ s, target GV1 (dark circle) is tracked by UA1 and UA4 (dark triangles) whereas GV2 (light circle) is tracked by UA5 and UA6 (light triangles). In the CSAT architecture presented here, UA do not attempt to maintain the specified separation to targets they have not been assigned, thus UA5 heads straight toward GV1 and passes within the stand-off radius around the target. Because UA5 is now closest to GV1, it is reassigned to track GV1 at time $t = 290$ s whereas UA1 is reassigned to GV2. As the hand off ends, UA4 and UA5 (now both dark triangles, indicating they are tracking the dark circle denoting GV1) phase themselves around GV1, whereas UA1 and UA6 phase themselves as they follow GV2.

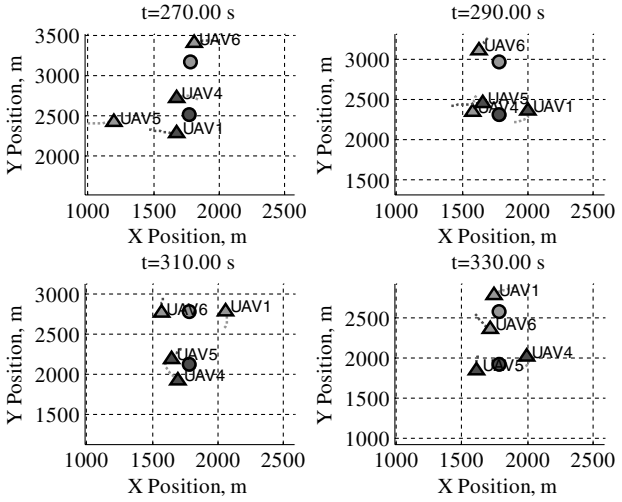

Fig. 19 Target hand off because of close proximity of UA to targets. Initially UA1 and UA4 (dark triangles) are assigned to track GV1 (dark circle), whereas UA6 and UA6 (light triangles) track GV2 (light circle). When UA5 approaches closely to GV1, it is reassigned to track it, whereas UA1 is reassigned to GV2.

V. Conclusions

This paper presented a cooperative stand-off line-of-sight tracking algorithm based on modified Lyapunov guidance vector fields that produce stable convergence to a circling limit cycle behavior.

Guidance vector fields were developed that yield feasible, globally stable paths with guaranteed target stand-off distance bounds. In addition to the global stability property, another benefit of the vector field approach presented here is that UA behavior converging toward the desired loiter pattern can be specified by the construction of the vector field, as opposed to stability-oriented approaches, which only specify the final path-following behavior. For example, the vector fields given here smoothly combine radial velocity components that dominate when the UA is located far from the stand-off distance with tangential components that dominate along the desired circular path. Because of the explicit separation between guidance and tracking control, the vector fields described here can be used as the outer guidance layer for many different types of vehicles whereas lower-level reference tracking control can be designed to meet the constraints of specific vehicles. Further extensions of the vector field approach are in progress and include applying diffeomorphisms that warp the loiter pattern into other closed curves whereas preserving global stability, stringing multiple loiter circles together to perform waypoint navigation, and hierarchical nesting of globally stable attractors for heterogeneous teams of vehicles.

A basic Lyapunov guidance vector field was exhibited, which works well for a single vehicle and a stationary target. This guidance law was shown to be robust to errors caused by uncertain target velocity and wind, and conservative bounds on the deviation from the desired tracking behavior were provided. If bounds on the speed of a constant-velocity target are known, the commanded radius can be increased to account for these bounds, and stand-off tracking beyond the desired distance can still be maintained. It was also shown how accurate estimates of target and wind velocities can be used to modify the algorithm to recover exact stand-off radius tracking.

Cooperative tracking by multiple unmanned aircraft was achieved through additional phasing around the desired orbit pattern. Differential speed commands were used to space cooperating vehicles around the specified circular path. Because the vector field reference tracking control only uses vehicle turn rate commands, phased spacing using speed variations was decoupled from stand-off tracking and global stability of the vector field was maintained. Like the vector fields, the differential speed commands were weighted according to the distance of the vehicles from the specified stand-off distance. Although stability to the desired loiter circle with desired phasing was proven for a stationary target without wind, the presence of either and typical constraints on aircraft speed can cause the relative phasing to oscillate. Convoy protection, in which the aircraft must scout an area ahead of the moving target, was performed by elongating the cooperative stand-off line-of-sight tracking limit cycle along the predicted target course.

Simulations evaluated the performance of the cooperative stand-off line-of-sight tracking algorithm in several realistic scenarios. Compared with the single-UA case, using the cooperative stand-off line-of-sight tracking algorithm with uniform (i.e., 180 deg apart relative to the target) phasing decreased the separation distance an evasive target was able to achieve from the UA team by at least 100 m. Furthermore, the results showed that the value of cooperation improves as the speed of the target approaches the speed of the aircraft. Likewise, cooperative convoy protection increased the size of the coverage area around a friendly ground target as it moved, increasing the distance at which adversarial targets could be detected, increasing the protection envelope around the friendly target, and decreasing the exposure to undetected threats. Finally, simulations of a more complex cooperative search, acquisition, and tracking scenario were described that relied on the cooperative stand-off line-of-sight and convoy protection controllers, as well as mode assignment by a higher level coordination control layer. This scenario illustrates that sophisticated overall capability can be obtained from well-behaved guidance layer controllers whose modes are orchestrated using simple optimization at the high level.

References

[1] Frew, E. W., and Lawrence, D., "Cooperative Stand-Off Tracking of Moving Targets by a Team of Autonomous Aircraft," *AIAA Guidance, Navigation, and Control Conference*, Vol. 7, AIAA, Reston, VA, 2005, pp. 4885–4895.

[2] Rysdyk, R., Lum, C., and Vagners, J., "Autonomous Orbit Coordination for Two Unmanned Aerial Vehicles," *AIAA Guidance, Navigation, and Control Conference*, Vol. 6, AIAA, Reston, VA, 2005, pp. 4876–4884.

[3] Park, S., Deyst, J., and How, J. P., "A New Nonlinear Guidance Logic for Trajectory Tracking," *AIAA Guidance, Navigation, and Control Conference*, Vol. 2, AIAA, Reston, VA, 2004, pp. 941–956.

[4] Spry, S., Vaughn, A., and Xiao, X., "A Vehicle Following Methodology for UAV Formations," *Theory and Algorithms For Cooperative Systems*, edited by D. A. Grundel, Panos M. Pardalos, and Robert Murphey, Series on Computers and Operations Research, World Scientific Publishing Company, Hackensack, New Jersey, pp. 513–534, Chap. 23.

[5] Frew, E., Spry, S., and McGee, T., "Flight Demonstrations of Self-Directed Collaborative Navigation of Small Unmanned Aircraft," *AIAA 3rd "Unmanned Unlimited" Technical Conference, Workshop and Exhibit*, Vol. 2, AIAA, Reston, VA, 2004, pp. 1108–1121.

[6] Spry, S. C., Girard, A. R., and Hedrick, J. K., "Convoy Protection Using Multiple Unmanned Aerial Vehicles: Organization and Coordination," *Proceedings of the 2005 American Control Conference*, Vol. 5, IEEE Publications, Piscataway, NJ, 2005, pp. 3524–9.

[7] Rysdyk, R., "Unmanned Aerial Vehicle Path Following for Target Observation in Wind," *Journal of Guidance, Control, and Dynamics*, Vol. 29, No. 5, 2006, pp. 1092–1100.

[8] Wise, R. A., and Rysdyk, R. T., "UAV Coordination for Autonomous Target Tracking," *AIAA Guidance, Navigation, and Control Conference and Exhibit*, Vol. 5, AIAA, Reston, VA, 2006, pp. 3210–3231.

[9] Barth, E. J., "A Cooperative Control Structure for UAVs Executing a Cooperative Ground Moving Target Engagement (CGMTE) Scenario," *Proceedings of the 2006 American Control Conference*, Vol. 2006, IEEE Publications, Piscataway, NJ, 2006, pp. 2183–2190.

[10] Justh, E. W., and Krishnaprasad, P. S., "Steering Laws and Continuum Models for Planar Formations," *42nd IEEE International Conference on Decision and Control*, Vol. 4, IEEE Publications, Piscataway, NJ, 2003, pp. 3609–14.

[11] Klein, D. J., and Morgansen, K. A., "Controlled Collective Motion for Trajectory Tracking," *Proceedings of the 2006 American Control Conference*, Vol. 2006, IEEE Publications, Piscataway, NJ, 2006, pp. 5269–5275.

[12] Sepulchre, R., Paley, D., and Leonard, N., "Collective Motion and Oscillator Synchronization," *Cooperative Control. A Post-Workshop Volume 2003 Block Island Workshop on Cooperative Control*, Springer–Verlag, New York, 2004, pp. 189–205.

[13] Paley, D., Leonard, N. E., and Sepulchre, R., "Oscillator Models and Collective Motion Splay State Stabilization of Self-Propelled Particles," *44th IEEE Conference on Decision and Control*, Vol. 2005, IEEE Publications, Piscataway, NJ, 2005, pp. 3935–3940.

[14] Waydo, S., and Murray, R. M., "Vehicle Motion Planning Using Stream Functions," *2003 IEEE International Conference on Robotics and Automation*, Vol. 2, IEEE Publications, Piscataway, NJ, 2003, pp. 2484–2491.

[15] Rimon, E., and Koditschek, D. E., "Exact Robot Navigation Using Artificial Potential Functions," *IEEE Transactions on Robotics and Automation*, Vol. 8, No. 5, 1992, pp. 501–518. doi:10.1109/70.163777

[16] Lawrence, D. A., "Lyapunov Vector Fields for UAV Flock Coordination," *2nd AIAA "Unmanned Unlimited" Conference and Workshop and Exhibit*, AIAA, Reston, VA, 2003.

[17] Nelson, D. R., Barber, D. B., McLain, T. W., and Beard, R. W., "Vector Field Path Following for Small Unmanned Air Vehicles," *IEEE Transactions on Robotics and Automation*, Vol. 23, No. 3, June 2007, pp. 519–529.

[18] Frew, E. W., "Sensitivity of Cooperative Geolocalization to Orbit Coordination," *AIAA Guidance, Navigation, and Control Conference*, AIAA, Reston, VA, Aug. 2007.

[19] Guldner, J., and Utkin, V. I., "Sliding Mode Control for an Obstacle Avoidance Strategy Based on a Harmonic Potential Field," *32nd IEEE Conference on Decision and Control*, Vol. 1, IEEE Publications, Piscataway, NJ, 1993, pp. 424–429.

[20] Leonard, N. E., and Fiorelli, E., "Virtual Leaders, Artificial Potentials, and Coordinated Control of Groups," *40th IEEE Conference on Decision and Control*, Vol. 3, IEEE Publications, Piscataway, NJ, 2001, pp. 2968–2973.

[21] Parunak, H., Van Dyke, Purcell, M., and O'Connell, R., "Digital Pheromones for Autonomous Coordination of Swarming UAVs," *1st AIAA Technical Conference and Workshop on UAV Systems, Technologies, and Operations*, AIAA, Reston, VA, 2002.

[22] Polycarpou, M. M., Yang, Y., and Passino, K. M., "A Cooperative Search Framework for Distributed Agents," *Proceedings of the IEEE International Symposium on Intelligent Control*, IEEE Publications, Piscataway, NJ, 2001, pp. 1–6.

[23] Yang, I. H., and Zhao, Y. J., "Real-Time Trajectory Planning for Autonomous Aerospace Vehicles Amidst Static Obstacles," *1st AIAA Technical Conference and Workshop on UAV Systems, Technologies, and Operations*, AIAA, Reston, VA, 2002.

[24] Ousingsawat, J., and Campbell, M. E., "Establishing Trajectories for Multi-Vehicle Reconnaissance," *AIAA Guidance, Navigation, and Control Conference*, Vol. 3, AIAA, Reston, VA, 2004, pp. 2188–2199.

[25] Lawrence, D., Mohseni, K., and Han, R., "Information Energy for Sensor-Reactive UAV Flock Control," *AIAA 3rd "Unmanned Unlimited" Technical Conference, Workshop and Exhibit*, Vol. 2, AIAA, Reston, VA, 2004, pp. 631–644.

[26] Dixon, C., and Frew, E., "Maintaining a Linked Network Chain Utilizing Decentralized Mobility Control," *AIAA Guidance, Navigation, and Control Conference and Exhibit*, Vol. 5, AIAA, Reston, VA, 2006, pp. 3338–3345.

[27] Khalil, H. K., *Nonlinear Systems*, 3rd ed., Prentice–Hall, Upper Saddle River, NJ, 2002, Chaps. 2–3.

[28] Lawrence, D., Frew, E., and Pisano, W., "Lyapunov Vector Fields for Autonomous UAV Flight Control," *AIAA Guidance, Navigation, and Control Conference*, AIAA, Reston, VA, August 2007.

[29] Osborne, J., and Rysdyk, R., "Waypoint Guidance for Small UAVs in Wind," *Proceedings of the AIAA Infotech@Aerospace Conference*, Vol. 1, AIAA, Reston, VA, 2005, pp. 459–470.

[30] Dogan, A., and Zengin, U., "Unmanned Aerial Vehicle Dynamic-Target Pursuit by Using Probabilistic Threat Exposure Map," *Journal of Guidance, Control, and Dynamics*, Vol. 29, No. 4, 2006, pp. 944–954.